A Draft of PAC42 Hall A Proposal

Measurements of SIDIS Double-Spin Asymmetries on a Longitudinally Polarized ^{3}He Target

(Draft version as of May 15, 2014.)

LANL folks + UConn Folks+SBS Collaborators

Xiaodong Jiang
Los Alamos National Laboratory

Andrew Puckett
University of Connecticut

This is a working draft.

Abstract

Precision measurements of longitudinal double-spin asymmetries A_{1h}^n, $h = \pi^+, \pi^-, \pi^0, K^+, K^-$ in semi-inclusive deep-inelastic scattering on a longitudinally polarized ^{3}He target are proposed. These asymmetries are sensitive to the flavor-separated quark helicity distributions of the nucleon. The flavor decomposition of nucleon spin is one of the major physics goals of the JLab 12 GeV upgrade. The experiment will reach high statistical figure-of-merit using a high-luminosity polarized ^{3}He target and the BigBite and Super BigBite spectrometers in Hall A, in a configuration identical to approved experiment E12-09-018, that will measure transverse single-spin asymmetries in SIDIS. Compared to existing and planned measurements on proton and deuteron targets, SIDIS asymmetries measured on ^{3}He provide superior sensitivity to Δd and $\Delta \bar{d}$. The kaon SIDIS asymmetries measured by this experiment will provide access to the polarized strange quark distribution Δs. A total of 30 days of running in Hall A are requested, including 20 days at 11 GeV and 10 days at 8.8 GeV. The proposed experiment will dramatically improve our knowledge of the flavor-separated quark helicity distributions in the valence region, and provide precision data for the next generation of NLO QCD global analysis of polarized PDFs.

Contents

Chapter 1

Executive Summary

Nucleon spin-flavor decomposition is one of the main questions facing our field, and is one of the key physics program that have driven the JLab-12 GeV upgrade.

The physics goals of this experiment includes:

- Provide the highest precision data set of polarized neutron (^{3}He) double-spin asymmetry A_{1n}^h in several hadron production channels in semi-inclusive Deep-Inelastic Scattering reactions, with hadron $h = \pi^+, \pi^-, \pi^0, K^+, K^-$, on a dense grid, over a wide range of (x, Q^2, z) and also cover a wide range of hadron transverse momentum p_T^h.

- Investigate the behavior of A_{1n}^h on its dependency of Q^2, z, hadron p_T^h and azimuthal angle ϕ_h. Compare with the expected behavior from Next-Leading-Order QCD predictions, identify possible higher-twist effects

- Through the method of Next-Leading-Order (NLO) QCD global fit , obtain the best knowledge of nucleon spin-flavor decomposition. Provide clear answers to the questions: Are sea quarks polarized ? Do anti-up quarks carry positive helicity as STAR W asymmetry data indicated ? How much helicity each quark flavor carry ?

- Through the method of Leading-Order "Purity Method" obtain 5-flavor nuclear spin decomposition, as applied in HERMES and COMPASS data, obtain ratios of $\Delta q/q$ for each quark flavor $[\Delta u/u, \Delta d/d, \Delta\bar{u}/\bar{u}, \Delta\bar{d}/\bar{d}$ and $(\Delta s + \Delta\bar{s})/(s + \bar{s})]$.

- Through deliberate careful control of phase space and detection efficiency, obtain high precision results on the charged pion difference asymmetry, $A_{1n}^{\pi^+ - \pi^-}$, a charge and flavor non-singlet observable which is only sensitive to valence quark polarization $\Delta d_v - 1/4\delta u_v$. When combined with future JLab SIDIS data on a polarized proton target, obtain Δu_v, Δd_v and polarized sea flavor asymmetry $\Delta\bar{u} - \Delta\bar{d}$, and their fist moments, such as $\int[\Delta\bar{u}(x) - \Delta\bar{d}(x)]dx$.

- Through high precision SIDIS hadron multiplicity data within the same experimental set up, on unpolarized reference cell runs, carry out a self-consistent simultaneous NLO fit on multiplicity and spin asymmetry to constrain fragmentation function and parton helicity. High precision results from this experiment will build up into a JLab-12 GeV SIDIS database for future NLO fits, which will also include data from polarized proton and deuteron targets.

This proposal follows the footsteps of earlier JLab-6GeV spin-flavor decomposition proposals and an earlier JLab-12 GeV proposal. Using the same high luminosity polarized ^{3}He target system and two large acceptance spectrometer combination: BigBite Spectrometer as the electron arm and

Super-BigBite Spectrometer (SBS) as the hadron arm, as in the approved Transversity experiment, this experiment will be able to collect data in the same run group as the Transversity experiment, with a longitudinal target spin setting. The main features of this experiment includes:

- World highest luminosity polarized target (^{3}He), with an average polarization of 65%.
- Two large acceptance magnetic spectrometers, as electron-arm and hadron-arm detect SIDIS in coincidence. The best Figure-Of-Merit for neutron SIDIS spin asymmetries.
- The highest Q^2 available for SIDIS reactions at JLab-12 GeV, completely complimentary to that of the SoLID experiment in Hall A. At beam energies of 11 GeV and 8.8 GeV, provide coverage to a wide range of Q^2 , similar to that of CLAS12.
- Clear particle identification and reliable separation of π/K over the entire range of hadron momentum through the Ring Imaging Cherenkov detector in SBS.
- Identical detection phase space for positively-charged and negatively-charged hadrons, and through SBS magnetic field reversal, a unique feature that is ideal to measure SIDIS yield differences of $\pi^+ - \pi^-$ and corresponding asymmetries.

Chapter 2

Introduction and Physics Motivation

2.1 Introduction

The last two decades has seen remarkable progress in the knowledge of the polarized parton distribution functions (pPDF) $\Delta q_f(x)$. The most precise and clearly interpreted data are from inclusive deep-inelastic lepton scattering (DIS) experiments at CERN and SLAC. However, the information available from inclusive DIS process has inherent limitations. As the cross sections are only sensitive to e_q^2, the quark charge square, an inclusive experiment probes quarks and anti-quarks on an equal footing, and it is only possible to determine combinations of $\Delta q + \Delta\bar{q}$, but never the valence $\Delta q_v = \Delta q - \Delta\bar{q}$ nor the sea $\Delta\bar{q}$ separately. Therefore it is not sensitive to the symmetry breaking in the sea sector. Through inclusive DIS measurements, only one particular flavor non-singlet can be directly inferred i.e. $\Delta q_3(x, Q^2) = \Delta u + \Delta\bar{u} - \Delta d - \Delta\bar{d}$. The additional assumption of $\mathrm{SU}(3)_f$ flavor symmetry allows the hyperon beta decay data to constrain the first moments of Δq. The well-cited result of this approach is that quark helicities seem to make a small net contribution to the nucleon spin, and the strange sea appears to be negatively polarized.

Is sea quark polarized ? This question has been tantalizing us for the last two decades. very recently, from RHIC STAR experiment's W-boson spin asymmetry measurements [1], as shown in Fig 2.1, the data strongly favor a positively polarized sea up-quark.

The sensitivity to each individual quark flavor can also be realized in semi-inclusive deep inelastic scattering (SIDIS) in which one of the leading hadrons in quark fragmentation is also detected. Since the leading hadrons from the current fragmentation carry information about the struck quark's flavor, detection of the leading hadron effectively "tags" the quark flavor. Therefore, SIDIS offers an unique opportunity for determining the spin, flavor, and sea structure of the nucleon [**?**], thereby significantly enriching our understanding of QCD and the nucleon structure. High precision polarized SIDIS data on the proton and the neutron (in a deuteron or a ^{3}He nuclei) allows a flavor decomposition of nucleon spin structure, which could lead to the discovery of a possible flavor-asymmetry in the polarized sea. A decade ago, in 2005, the HERMES collaboration published the results of a leading order spin flavor decomposition from polarized proton and deuteron data, and for the first time extracted the sea quark polarizations [**?**, **?**]. Unlike the predictions of several theoretical models, HERMES data indicated that within the available statistics $\Delta\bar{u} - \Delta\bar{d}$ is consistent with an unbroken $\mathrm{SU}(2)_f$ symmetry. These results have been confirmed in 2011 by the COMPASS Collaboration.

The HERMES data demonstrated that, within the experimental precision, the semi-inclusive double-spin asymmetries A_{1N}^h at $\langle Q^2\rangle = 2.5$ GeV^2 agree reasonably well with the SMC data [**?**] at $\langle Q^2\rangle = 10$ GeV^2, COMPASS asymmetry data on deuteron [**?**], an proton targets averaged at

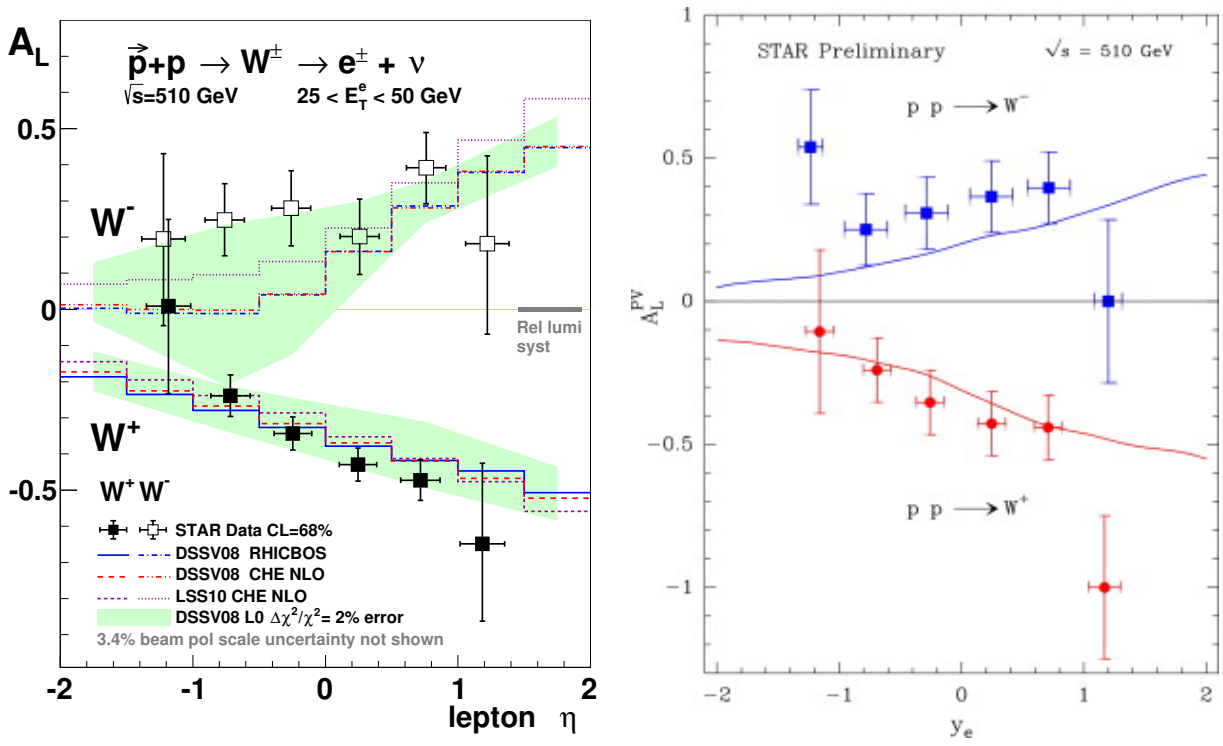

Figure 2.1: (left)Recent results from STAR, longitudinal single-spin asymmetry, A_L, for $W^{\pm}$ production as a function of lepton pseudorapidity, η_e, in comparison to theory predictions. (right need replaced) BBS2008 prediction compared with STAR preliminary data.

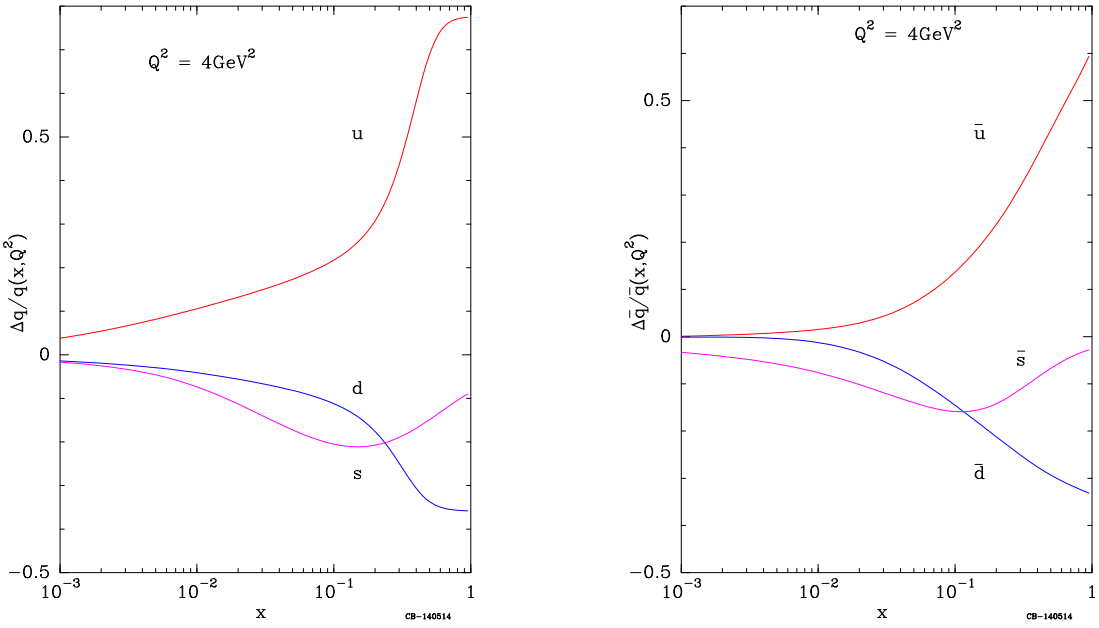

Figure 2.2: BBS2008 prediction of raio for different quark flavor $\Delta q/q$ (left) and $\Delta\bar{q}/\bar{q}$ at the kinematics of this experiment $Q^2 = 4.0$ GeV^2.

$\langle Q^2 \rangle = 10$ GeV^2, was also shown to agree well with HERMES data.

This non-trivial agreement indicates that semi-inclusive asymmetries have rather weak Q^2 dependencies and the expected violation of naive leading order x-z separation is not large. The apparent "precocious scaling" suggests that at a modest Q^2, such as at HERMES $\langle Q^2 \rangle = 2.5$ GeV^2 and at $\langle Q^2 \rangle = 4.0$ GeV^2 for this experiment, information on the quark distributions should be reasonably well-preserved in semi-inclusive reactions. Ji, Ma and Yuan have explicitly proved [**?**] that QCD factorization is valid for SIDIS with hadrons emitted in the current fragmentation region with low transverse momentum $p_{\perp h} \ll Q$. QCD factorization of spin-dependent cross sections in SIDIS and Drell-Yan has also been proved for the low $p_{\perp h}$ case [**?**]. JLab E00-108 data [**?**], on unpolarized SIDIS cross section ratios of proton and deuteron with 5.5 GeV beam and $\langle Q^2 \rangle = 2.3$ GeV^2, also indicated that the leading order naive x-z separation is rather close to the reality.

It was pointed out by Frankfurt et al. [**?**] and by Christova and Leader [**?**] that if the yield-difference helicity-asymmetries $A_{1N}^{\pi^+ - \pi^-}$ are measured with high precision, quark polarization Δu_v, Δd_v and $\Delta \bar{u} - \Delta \bar{d}$ can be extracted at leading order independent of the knowledge of fragmentation functions. Even at the next-to-leading order, information on the valence quark polarizations is well-preserved in the combined asymmetries $A_{1N}^{\pi^+ - \pi^-}$, due to the fact that contributions from gluons as well as sea-quarks cancel exactly to all orders of QCD [**?**] in this charge and flavor non-singlet combination. In practice, the combined asymmetry $A_{1N}^{\pi^+ - \pi^-}$ poses more experimental challenges, since precise knowledge on hadron phase spaces and detection efficiencies are required. This experiment is specifically designed to measure $A_{1N}^{\pi^+ - \pi^-}$. Different from other SIDIS measurements like HERMES and COMPASS, this experiment will use two independent magnetic spectrometers. By flipping the magnetic polarity of the hadron spectrometer, identical phase spaces between π^+ and π^- reaction can be achieved such that the combined asymmetry $A_{1He}^{\pi^+ - \pi^-}$ can be determined with high precision. At Q^2 of $2.0 \sim 6.7$ GeV^2, and $x = 0.110 \sim 0.600$??? xxx.xx , this experiment will provide independent precision data on $\Delta d_v - \frac{1}{4}\Delta u_v$. When combined with the expected world data on polarized proton, to obtain $\Delta u_v - \Delta d_v$, this experiment will provide the opportunity to address the polarized sea asymmetry $\Delta \bar{u} - \Delta \bar{d}$.

At the next-to-leading order, following the well established formalism [**?**], tools of NLO QCD global fits, which include data sets from both inclusive and semi-inclusive reactions, have become available. As a standard procedure, such global NLO QCD fit has also included RHIC pp data [**?**], in forward π^0 and jet longitudinal double-spin asymmetries $A_{LL}^{\pi^0}$, and A_{LL}^{jet}. Although there's a reasonable set of SIDIS data on proton and deuteron targets, from HERMES and COMPASS experiment, and soon from JLab-6GeV CLAS eg1-dvcs run group, the world data on SIDIS asymmetries currently only includes one ^{3}He data set, with rather large error bars, obtained by HERMES in 1996. The high statistics ^{3}He data from this experiment, adding much precise neutron SIDIS asymmetries to the world data sample, will serve as stringent constraints on pPDFs through NLO global fits [**?**]. Data from this experiment will indirectly constrain Δg through NLO global fit. The main source of this sensitivity to Δg comes from the Q^2-evolutions of the inclusive g_1 structure function, but now with sea and valence contributions much better separated by semi-inclusive data in the global fit [**?**, **?**]. Therefore, data from this experiment will independently verify the recent claim of a small positive gluon polarization based on RHIC inclusive jet data.

Jefferson Lab Hall A, with its high luminosity polarized ^{3}He target, has the unique advantage in providing high precision neutron asymmetry data in nucleon spin studies. In obtaining quark helicity information from neutron, the Figure-of-Merit of a polarized ^3He target has always been much better than from that of a polarized deuteron target from ND_3. For example, Hall A data on inclusive A_{1n} and g_2^n measurements [**?**, **?**] has improved previous world knowledge by an order of magnitude in each case. The Hall A polarized ^{3}He target system has been under continuous

improvements over the last decade. Recently, it reached an average in-beam polarization of 60% during the Neutron Transversity experiment (E06-010). A large acceptance magnetic spectrometer, the BigBite spectrometer, with its electron detector package has been operated successfully in Neutron Transversity and d2n experiments. The planned Hall A Super-Big-Bite spectrometer with a large solid angle and a large momentum acceptance, in addition to its unique particle identification Ring Imaging Chrecnkov detector (RICH), in combination with the high polarization electron beam at 11 GeV, a high luminosity and high polarization ^{3}He target, make it possible for a dramatic improvement on the world data set of SIDIS neutron asymmetries.

2.2 Physics Motivation

The principle goal of spin-dependent SIDIS experiments is to perform flavor decomposition of nucleon spin structure taking advantage of flavor tagging. In this section, we first express the SIDIS cross sections and asymmetries at leading order (LO) and summarize the HERMES results of "purity method" (more details in Appendix). After introducing the next-to-leading order cross sections, we summarize the NLO global QCD analysis method. We will then outline new methods of flavor decomposition: the Christova-Leader method at leading order and next-to-leading order. Theoretical models of polarized light sea asymmetry $\Delta\bar{u}-\Delta\bar{d}$ is summarized at the end. Throughout this proposal, SU(2) isospin symmetry and charge conjugation invariance are assumed and heavy quark contributions are neglected.

2.2.1 Beam-target double-spin asymmetries at leading order

At the leading order, the SIDIS process is separated into a hard-scale quark scattering followed by a soft-scale hadronization. The "naive x-z separation" assumption, on which the SMC and HERMES analysis were based, implies that the spin-independent (σ^h) and the spin-dependent ($\Delta\sigma^h$) cross sections follow:

$$\sigma^h(x,z) = \sum_f e_f^2 q_f(x)\cdot D_{q_f}^h(z), \qquad \Delta\sigma^h(x,z) = \sum_f e_f^2 \Delta q_f(x)\cdot D_{q_f}^h(z), \tag{2.1}$$

where $x = Q^2/2M\nu$, $z = E_h/\nu$. The fragmentation functions $D_{q_f}^h(z)$ represent the probability that a quark f fragments into a hadron h.

Considering the beam and target polarization (P_B and P_T), and the dilution factor ($f^h = \sigma^h_{pol.N}/\sigma^h_{allN}$), which accounts for the unpolarized nucleons in the target, the double-spin asymmetry [**?**] for a longitudinally polarized beam on a longitudinally polarized target is :

$$A_\parallel^h = f^h P_B P_T \cdot \mathcal{P}_{kin}\cdot A_{1N}^h, \tag{2.2}$$

the kinematic factor $\mathcal{P}_{kin}$ is:

$$\mathcal{P}_{kin} = \mathcal{D}\cdot(1+\gamma\eta)\cdot\frac{1+R}{1+\gamma^2}, \tag{2.3}$$

in which

$$\begin{aligned} \eta &= \frac{2\gamma(1-y)}{2-y}, \qquad\qquad \mathcal{D} = \frac{1-(1-y)\epsilon}{1+\epsilon\cdot R}, \\ \epsilon^{-1} &= 1+2(1+\nu^2/Q^2)\tan^2(\theta_e/2), \end{aligned} \tag{2.4}$$

$\mathcal{D}$ is the virtual photon polarization, $R(x,Q^2) = \sigma_L/\sigma_T$ accounts for the longitudinal component of the virtual photon and $y = \nu/E_0$, $\gamma^2(x,Q^2) = 4M^2x^2/Q^2$. In the current fragmentation regime, the virtual photon asymmetry is defined as:

$$A_{1N}^h(x,Q^2,z) \equiv \frac{\Delta\sigma^h(x,Q^2,z)}{\sigma^h(x,Q^2,z)} = \frac{\sum_f e_f^2 \Delta q_f(x,Q^2)\cdot D_{q_f}^h(z,Q^2)}{\sum_f e_f^2 q_f(x,Q^2)\cdot D_{q_f}^h(z,Q^2)}. \tag{2.5}$$

Each individual measurement on $A_{1N}^h(x,Q^2,z)$ provides an independent constrain on the polarized parton distributions $\Delta q_f(x,Q^2)$. Data from HERMES on proton and deuteron, and from COMPASS on deuteron target are summarized in Appendix-A.

In principle, the asymmetry A_{1N}^h depends on both variables x and z, its x-dependency comes from parton distributions and z-dependency comes from fragmentation functions. Generally speaking, accurate knowledge of the fragmentation functions is crucial in order to extract quark polarizations from the measured asymmetries according to Eq. 2.5. However, in some special combinations, if σ^h and $\Delta\sigma^h$ happen to have similar z-dependencies, as their ratio, the asymmetry will end up with a weak or even vanishing z-dependency. This type of cancellation can provide us with much cleaner observables to access quark polarizations without the complication of fragmentation functions. For example, Christova and Leader pointed out [**?**] that at the leading order, under the assumptions of SU(2) isospin symmetry and charge conjugation invariance, the fragmentation functions canceled exactly in the combined $h^+ \pm h^-$ double-spin asymmetries. Furthermore, if strange quark contribution can be neglected, the semi-inclusive asymmetry $A_{1N}^{\pi^+ + \pi^-}$ is reduced to the inclusive asymmetry A_{1N}. Indeed, at the next-to-leading order, the z-dependence of $A_{1N}^{\pi^+ \pm \pi^-}$ is predicted to be very small [**?**].

2.2.2 HERMES results from leading order purity method

The HERMES result of flavor decomposition [**?**] is shown in Fig. 2.3. As expected, u-quarks are strongly polarized in the direction of proton spin, while d-quarks are polarized opposite to the proton spin. The sea quark polarizations are consistent with zero. Fig. 2.3 right panel shows the HERMES result of $x(\Delta\bar{u} - \Delta\bar{d})$ together with predictions of a broken $\mathrm{SU}(2)_f$ symmetry [**?**, **?**]. The data are consistent with an unbroken $\mathrm{SU}(2)_f$ sea symmetry.

Figure 2.3: The HERMES result [**?**] of polarized quark distribution $x\cdot\Delta q(x)$ for u, $\bar{u}$, d, $\bar{d}$, and $s+\bar{s}$ versus x in comparison with two different parametrizations [**?**, **?**] is shown on the left. The difference of the polarized light sea $x(\Delta\bar{u} - \Delta\bar{d})$ is shown on the right. The error bars are statistical, while the shaded bands at the bottom indicate the systematic uncertainties.

The HERMES results left much room for improvement, with respect to statistical accuracies, especially on $\Delta\bar{u} - \Delta\bar{d}$. In addition, the validity and the stability of the leading order purity method needs to be independently verified. As pointed out by many authors, the issue of leading order violation of naive x-z separation and the intrinsic uncertainties of the fragmentation Monte Carlo simulation need to be quantitatively addressed at a level appropriate to the sea contribution [**?**].

2.2.3 Neutron SIDIS asymmetries are sensitive to Δd and $\Delta\bar{d}$

For a proton and a deuteron target, one expects u-quark dominates in SIDIS cross section due to e_q^2 weighting, as in the case of HERMES and COMPASS data. However, one expects Δd to be better constrained by neutron data from a polarized ^{3}He target. In Fig. **??**, the fractional contribution of

each quark flavor to the SIDIS cross sections σ_q^h/σ_{all} are shown for proton (left panel) and neutron (right panel), that is:

$$\frac{\sigma_q^h}{\sigma_{all}} = \frac{e_q^2 \cdot q(x,Q^2) \cdot D_q^h(z,Q^2)}{\sum_f e_f^2 \cdot q_f(x,Q^2) \cdot D_f^h(z,Q^2)}. \tag{2.6}$$

Sensitivities to d and $\bar{d}$ contributions in the neutron SIDIS cross sections are clearly demonstrated. The HERMES collaboration collected limited polarized ^{3}He data back in 1996, which formed the basis of its first flavor decomposition paper [**?**].

2.2.4 SIDIS Cross sections at the next-to-leading order

The naive x-z separation is no longer valid at the next-to-leading order when gluon diagrams in Fig. **??** are considered. However, the exact form of the NLO cross section has been well-known [**?**]. At NLO, the terms of $q(x)\cdot D(z)$ and $\Delta q(x)\cdot D(z)$ in Eq. 2.1 are added with the double convolutions of the type $q\otimes\mathcal{C}\otimes D$ and $\Delta q\otimes\Delta C\otimes D$ in which $\mathcal{C}$ and ΔC are well-known Wilson coefficients [**?**]:

$$[q\otimes C\otimes D](x,z) = \int_x^1 \frac{dx'}{x'}\int_z^1 \frac{dz'}{z'} q\left(\frac{x}{x'}\right) C(x',z') D\left(\frac{z}{z'}\right). \tag{2.7}$$

We define the short-hand notation:

$$qD + \frac{\alpha_s}{2\pi} q\otimes C\otimes D = q\left[1+\otimes\frac{\alpha_s}{2\pi}C\otimes\right] D, \tag{2.8}$$

at NLO instead of Eq. 2.1, we have:

$$\begin{aligned}
\sigma^h(x,z) &= \sum_f e_f^2 q_f \left[1+\otimes\frac{\alpha_s}{2\pi}\mathcal{C}_{qq}\otimes\right] D_{q_f}^h \\
&+ \left(\sum_f e_f^2 q_f\right)\otimes\frac{\alpha_s}{2\pi}\mathcal{C}_{qg}\otimes D_G^h + G\otimes\frac{\alpha_s}{2\pi}\mathcal{C}_{gq}\otimes\left(\sum_f e_f^2 D_{q_f}^h\right), \qquad (2.9)\\
\Delta\sigma^h(x,z) &= \sum_f e_f^2 \Delta q_f \left[1+\otimes\frac{\alpha_s}{2\pi}\Delta C_{qq}\otimes\right] D_{q_f}^h \\
&+ \left(\sum_f e_f^2 \Delta q_f\right)\otimes\frac{\alpha_s}{2\pi}\Delta C_{qg}\otimes D_G^h + \Delta G\otimes\frac{\alpha_s}{2\pi}\Delta C_{gq}\otimes\left(\sum_f e_f^2 D_{q_f}^h\right). \qquad (2.10)
\end{aligned}$$

It is also well-known that in the Mellin-n space, the double-convolutions factorize into simple products under moments, and the parton distributions can be recovered by an inverse Mellin transformation with all moments of Wilson coefficients already calculated [**?**].

2.2.5 NLO global QCD analysis of DIS and SIDIS data

At the next-to-leading order, the cross sections in Eq. 2.5 are replaced by Eq. 2.9 and Eq. 2.10. Following the well established [**?**] formalism, tools of NLO QCD global fits, which include data sets from inclusive and semi-inclusive reactions as well as pp data, have become available [**?**, 2], and the uncertainties of the pPDF can be addressed in the global fits. With the HERMES results, the polarized SIDIS data have a non-negligible weight in the combined global analysis, comparable to that of inclusive data. It helped to constrain the sea quark and gluon polarization complementing the information obtained from DIS. The NLO global fit [**?**] to the existing DIS and SIDIS data are shown in Fig. **??** in Appendix.

The precision data from this experiment, adding the neutron asymmetries to the world data, will serve as stringent constraints on pPDFs through NLO global fits [**?**]. The impacts on pPDF moments are presented in the result section. Since the combined asymmetries $A_{1n}^{\pi^+-\pi^-}$ are also measured in this experiment, the result of the NLO global fit can be cross checked with that from the NLO Christova-Leader method.

2.2.6 Method of spin-flavor decomposition

LO Christova-Leader method to obtain $\Delta u_v(x)$, $\Delta d_v(x)$ and $\Delta\bar{u}(x) - \Delta\bar{d}(x)$

At the leading order, under isospin symmetry and charge conjugation invariance, the fragmentation functions cancel exactly in the combined asymmetry $A_{1N}^{\pi^+\pm\pi^-}$. In addition, higher-twist terms in the fragmentation functions are also expected to be largely canceled [**?**]. In the quantities related to $\sigma^{\pi^+} - \sigma^{\pi^-}$ which is a charge and flavor non-singlet combination, sea-quarks and gluons do not contribute at any QCD-order [**?**].

From the Appendix, at leading order , for polarized protons, polarized deuterons and polarized neutrons [1] (in ^{3}He), we have:

$$A_{1p}^{\pi^+-\pi^-}(\vec{p}) = \frac{\Delta\sigma_p^{\pi^+} - \Delta\sigma_p^{\pi^-}}{\sigma_p^{\pi^+} - \sigma_p^{\pi^-}} = \frac{4\Delta u_v - \Delta d_v}{4u_v - d_v}, \tag{2.11}$$

$$A_{1d}^{\pi^+-\pi^-}(\vec{p}+\vec{n}) = \frac{\Delta\sigma_d^{\pi^+} - \Delta\sigma_d^{\pi^-}}{\sigma_d^{\pi^+} - \sigma_d^{\pi^-}} = \frac{\Delta u_v + \Delta d_v}{u_v + d_v}, \tag{2.12}$$

$$A_{1He}^{\pi^+-\pi^-}(\vec{n}+2p) = \frac{\Delta\sigma_{He}^{\pi^+} - \Delta\sigma_{He}^{\pi^-}}{\sigma_{He}^{\pi^+} - \sigma_{He}^{\pi^-}} = \frac{4\Delta d_v - \Delta u_v}{7u_v + 2d_v}. \tag{2.13}$$

Measurements on three different targets will over-determine Δu_v and Δd_v. Proton and deuteron measurements are more sensitive to Δu_v, measurements on ^{3}He are more sensitive to Δd_v. One can re-write the last relation as:

$$(\Delta d_v - \tfrac{1}{4}\Delta u_v)_{LO} = \frac{1}{4}(7u_v + 2d_v)\, A_{1He}^{\pi^+-\pi^-}. \tag{2.14}$$

This method of flavor decomposition involves helicity asymmetries of cross section differences. Kinematics need to be carefully chosen such that π^+ and π^- cross sections are reasonably different. Error propagation on $A_{1N}^{\pi^+-\pi^-}$ make this method unfavorable when π^-/π^+ ratio approaches unity. Fig. **??** in Appendix illustrates this point by comparing the purity method with the Christova-Leader method for HERMES data [**?**].

We can obtain the leading order quantity $\Delta u_v - \Delta d_v$ from combinations of either proton and ^{3}He data or proton and deuteron data as:

$$(\Delta u_v - \Delta d_v)_{LO} = \frac{1}{5}\left[\left(4u_v - d_v)A_{1p}^{\pi^+-\pi^-} - (7u_v + 2d_v)A_{1He}^{\pi^+-\pi^-}\right)\right], \tag{2.15}$$

$$(\Delta u_v - \Delta d_v)_{LO} = \frac{1}{5}\left[2\left(4u_v - d_v)A_{1p}^{\pi^+-\pi^-} - 3(u_v + d_v)A_{1d}^{\pi^+-\pi^-}\right)\right]. \tag{2.16}$$

On the other hand, constrained by the inclusive data, the flavor non-singlet quantity at all QCD orders is:

$$\Delta q_3(x, Q^2) \equiv (\Delta u + \Delta\bar{u}) - (\Delta d + \Delta\bar{d}). \tag{2.17}$$

[1] After the effective neutron polarization (86.5%) in ^{3}He is taken into account and the correction corresponding to the small proton polarization (2.8%) is applied.

The polarized sea asymmetry at all QCD orders is:

$$\Delta\bar{u} - \Delta\bar{d} = \frac{1}{2}\Delta q_3 - \frac{1}{2}(\Delta u_v - \Delta d_v). \tag{2.18}$$

At the leading order, we have:

$$\Delta q_3(x,Q^2)|_{LO} = 6\left[g_1^p(x,Q^2) - g_1^n(x,Q^2)\right], \tag{2.19}$$

$$\left[\Delta\bar{u}(x) - \Delta\bar{d}(x)\right]_{LO} = 3\left[g_1^p(x) - g_1^n(x))\right] - \frac{1}{2}(\Delta u_v - \Delta d_v)|_{LO}. \tag{2.20}$$

NLO Christova-Leader method

At the next-to-leading order, under isospin symmetry and charge conjugation invariance, the NLO convolution terms become much simpler in quantities that are related to $\sigma^{\pi^+} - \sigma^{\pi^-}$. Since the gluon-related terms are identical for π^+ and π^- production, they drop out in the differences [**?**]:

$$A_{1p}^{\pi^+-\pi^-}(\vec{p}) = \frac{(4\Delta u_v - \Delta d_v)\left[1 + \otimes(\alpha_s/2\pi)\Delta C_{qq}\otimes\right](D^+ - D^-)}{(4u_v - d_v)\left[1 + \otimes(\alpha_s/2\pi)\mathcal{C}_{qq}\otimes\right](D^+ - D^-)}, \tag{2.21}$$

$$A_{1d}^{\pi^+-\pi^-}(\vec{p}+\vec{n}) = \frac{(\Delta u_v + \Delta d_v)\left[1 + \otimes(\alpha_s/2\pi)\Delta C_{qq}\otimes\right](D^+ - D^-)}{(u_v + d_v)\left[1 + \otimes(\alpha_s/2\pi)\mathcal{C}_{qq}\otimes\right](D^+ - D^-)}, \tag{2.22}$$

$$A_{1He}^{\pi^+-\pi^-}(\vec{n}+2p) = \frac{(4\Delta d_v - \Delta u_v)\left[1 + \otimes(\alpha_s/2\pi)\Delta C_{qq}\otimes\right](D^+ - D^-)}{(7u_v + 2d_v)\left[1 + \otimes(\alpha_s/2\pi)\mathcal{C}_{qq}\otimes\right](D^+ - D^-)}. \tag{2.23}$$

in which Δu_v and Δd_v evolve as non-singlets and do not mix with sea-quark and gluon densities. Therefore, measurements of $A_{1N}^{\pi^+-\pi^-}$ can determine Δu_v and Δd_v at the next-to-leading order without any consideration of gluon and sea distributions. The double-convolution terms in Eq. 2.21 are expected to introduce negligible z-dependency in $A_{1N}^{\pi^+-\pi^-}$ at the kinematics of this experiment, as demonstrated in calculation of de Florian, Navarro and Sassot [**?**].

The first moment of $\Delta u_v - \Delta d_v$ is related to the moment of $\Delta\bar{u} - \Delta\bar{d}$ through the Bjorken sum rule at all orders of QCD [**?**]. The Bjorken sum rule, written in terms of the moment $\Delta_1 q = \int_0^1 dx \Delta q$,

$$\begin{aligned}\Delta_1 q_3 &\equiv \left[\Delta_1 u(Q^2) + \Delta_1\bar{u}(Q^2)\right] - \left[\Delta_1 d(Q^2) + \Delta_1\bar{d}(Q^2)\right] \\ &= \left|\frac{g_A}{g_v}\right| = 1.2670 \pm 0.0035 \;\; valid \;\; in\; all\; QCD\; orders.\end{aligned} \tag{2.24}$$

Therefore, valid in all QCD orders, we have:

$$\int_0^1 (\Delta\bar{u} - \Delta\bar{d})dx = \frac{1}{2}\left|\frac{g_A}{g_v}\right| - \frac{1}{2}\int_0^1 (\Delta u_v - \Delta d_v)dx. \tag{2.25}$$

In other words, if one measures the valence quark moment $\Delta u_v - \Delta d_v$ precise enough, for example to $\delta\left[\Delta_1 u_v - \Delta_1 d_v\right] = \pm 0.05$, one cam pin down the polarized sea asymmetry, to $\delta\left[\Delta_1\bar{u} - \Delta_1\bar{d}\right] = \pm 0.025$, that's eight standard deviations from the prediction of Chiral Quark Soliton model.

A well-defined procedure has been given [**?**] to obtain the moment $\Delta_1 u_v - \Delta_1 d_v$ directly from the measured asymmetries $A_{1N}^{\pi^+-\pi^-}$ without first solving Eq. 2.21 point-to-point. The stability of this procedure has been demonstrated [**?**] using the HERMES-1999 data.

From the deuteron data alone, one can also form Γ_v, the first moment of $\Delta u_v + \Delta d_v$, and extract at leading order the moment:

$$\int_0^1 (\Delta\bar{u} + \Delta\bar{d})dx = 3\Gamma_1^N - \frac{1}{2}\Gamma_v + \frac{1}{12}a_8 \tag{2.26}$$

where Γ_1^N is the moment of$g_1^N = (g_1^p + g_1^n)/2$ from inclusive data, and $a_8 = 3F - D$ is from hyperon β-decays.

The recent COMPASS results [**?**] of $A_d^{h^+-h^-}$ are shown in Fig. **??**. The extracted valence quark polarization $x(\Delta u_v + \Delta d_v)$ and the running-x_{min} integral of $\Delta u_v + \Delta d_v$ are shown in Fig. **??**. The fact that the integral of $\Delta u_v + \Delta d_v$ is significantly different from that of assumption of a symmetrical polarized sea indicated that the sign of $\Delta\bar{u}$ is opposite to that of $\Delta\bar{d}$.

Cross check Δq_v with the upgraded RHIC

With the planned RHIC luminosity upgrade, Δq can be measured through $W^\pm$ decays [**?**]. Since the Q^2-evolutions of valence densities Δq_v are well understood in QCD, consistency cross checks can be made between JLab data at $\langle Q^2\rangle = 4.0$ GeV^2 and RHIC data at $Q^2 = M_W^2$.

Spin observables to check the leading order naive x-z separation

A schematic strategy of to test leading order naive x-z separation was suggested [**?**] which requires prior knowledge of neither fragmentation functions nor parton distributions. The experimental observables in this strategy is to make the combined double-spin asymmetry $A_{1N}^{\pi^+ + \pi^-}$. If leading order naive x-z separation holds perfectly, $A_{1N}^{\pi^+ + \pi^-}$ will turn out to be identical to the inclusive A_{1N} asymmetry due to the exact cancellation of the fragmentation functions in the asymmetry under charge conjugation invariance and isospin symmetry. Their difference, $A_{1N}^{\pi^+ + \pi^-} - A_{1N}$, gives a clear indication on the size of the next-to-leading-order terms which violate the naive leading order x-z separation.

Assume $\Delta s = \Delta\bar{s} \approx 0$, the fragmentation functions are canceled at the leading order in the combined asymmetry $A_{1N}^{\pi^+ + \pi^-}$, such that:

$$\begin{aligned}
A_{1p}^{\pi^+ + \pi^-}(x, Q^2, z) &= \frac{\Delta\sigma_p^{\pi^+} + \Delta\sigma_p^{\pi^-}}{\sigma_p^{\pi^+} + \sigma_p^{\pi^-}} = \frac{4(\Delta u + \Delta\bar{u}) + \Delta d + \Delta\bar{d}}{4(u + \bar{u}) + d + \bar{d}} \equiv A_{1p}(x, Q^2), \\
A_{1d}^{\pi^+ + \pi^-}(x, Q^2, z) &= \frac{\Delta\sigma_d^{\pi^+} + \Delta\sigma_d^{\pi^-}}{\sigma_d^{\pi^+} + \sigma_d^{\pi^-}} = \frac{\Delta u + \Delta d + \Delta\bar{u} + \Delta\bar{d}}{u + d + \bar{u} + \bar{d}} \equiv A_{1d}(x, Q^2), \\
A_{1n}^{\pi^+ + \pi^-}(x, Q^2, z) &= \frac{\Delta\sigma_n^{\pi^+} + \Delta\sigma_n^{\pi^-}}{\sigma_n^{\pi^+} + \sigma_n^{\pi^-}} = \frac{\Delta u + \Delta\bar{u} + 4(\Delta d + \Delta\bar{d})}{u + \bar{u} + 4(d + \bar{d})} \equiv A_{1n}(x, Q^2).
\end{aligned} \tag{2.27}$$

The combined asymmetry $A_{1N}^{\pi^+ + \pi^-}$ reduces to the inclusive asymmetry A_{1N} under the leading order naive x-z separation. The relation $A_{1N}^{\pi^+ + \pi^-}(x, Q^2, z) = A_1(x, Q^2)$ is a rather strong condition to satisfy, since the left-hand side involves the hadron observable z while the right-hand side doesn't. The deviation of $A_{1N}^{\pi^+ + \pi^-}$ from the inclusive A_{1N} asymmetry "effectively" measures the relative importance of the contribution from the next-to-leading order terms.

The HERMES experiment extracted the combined asymmetry $A_{1N}^{h+\bar{h}}$ as shown in Fig. **??** in comparison with the inclusive asymmetry A_{1N}. The near perfect agreement of $A_{1N}^{h+\bar{h}}$ with A_{1N} at $\langle Q^2\rangle = 2.5$ GeV^2 indicated that the next-to-leading order correction terms are small or mostly canceled in the asymmetries and the target fragmentation contribution has a negligible impact to the asymmetries. Even better agreements should be expected in this experiment at JLab-12GeV,

since the much higher luminosity allow reasonable statistics at larger scattering angle resulted in $\langle Q^2 \rangle = 4.0$ GeV^2 for this experiment. Once this agreement can be clearly demonstrated with high precision, parton polarizations can be reliably extracted through the leading order interpretation of SIDIS asymmetries.

2.2.7 $\Delta\bar{u} - \Delta\bar{d}$: the flavor asymmetry in the polarized sea

Fermilab experiment E866 reported measurements of the yield ratio of Drell-Yan muon pairs from an 800 GeV/c proton beam incident on hydrogen and deuterium [**?**, **?**]. The data suggested a significantly asymmetric light sea quark distribution over an appreciable range in x; the asymmetry $\bar{d}/\bar{u}$ peaked around $x = 0.18$, as shown in Fig. **??**. Furthermore, based on the E866 data and the CTEQ4M global-fit values of $\bar{u} + \bar{d}$, the values of $\bar{d}(x) - \bar{u}(x)$ were extracted, wit the moment $\int_0^1 \left[\bar{d}(x) - \bar{u}(x)\right] dx = 0.118 \pm 0.012$. Many theoretical models, including the meson cloud model, the chiral-quark model, the Pauli-blocking model, the instanton model, the chiral-quark soliton model and the statistical model, have been proposed to explain the $\bar{d}/\bar{u}$ asymmetry. These models can describe the $\bar{d} - \bar{u}$ reasonably well. However, they all have difficulties explaining the $\bar{d}/\bar{u}$ ratio at $x > 0.2$.

Since the unpolarized sea demonstrates a significant flavor asymmetry, one naively speculates a sizable flavor asymmetry also exists for the polarized sea in the same x-region. Indeed, many theory models have specific implications for the spin structure of the nucleon sea. For example, the Pauli-blocking model and the instanton model both predict a large asymmetry, $\int_0^1 [\Delta\bar{u}(x) - \Delta\bar{d}(x)]dx = \frac{5}{3} \cdot \int_0^1 [\bar{d}(x) - \bar{u}(x)]dx \approx 0.2$. In the chiral-quark soliton model, $\Delta\bar{u} - \Delta\bar{d}$ appears in leading-order (N_c^2) in a large N_c-expansion, while $\bar{d} - \bar{u}$ appears in the next-to-leading order (N_c). On the other hand, those meson cloud models which only include the π-meson predict $\Delta\bar{u} = \Delta\bar{d} = 0$ since the sea-quarks reside in a spin-0 π-meson. By considering a vector meson (ρ) cloud, non-zero sea polarization was predicted. A summary of theoretical predictions [**?**] of $I_\Delta = \int_0^1 [\Delta\bar{u}(x) - \Delta\bar{d}(x)]dx$ are given in Table. 2.1. If the flavor asymmetry of the polarized sea is indeed as large as the predictions of many models shown in Table. 2.1, it would imply that a significant fraction of the Bjorken sum, $\int_0^1 [g_1^p(x) - g_1^n(x)]dx$, comes from the flavor asymmetry of the polarized nucleon sea. The high statistics ^{3}He data from this experiment, together with the expected world proton data, will provide us with the first opportunity to discover the asymmetry in the polarized sea.

Model	I_Δ prediction	Authors and References
Meson cloud	0	Eichten *et al.* [**?**],
(π-meson)		Thomas [**?**]
Meson cloud	$\simeq -0.007$ to -0.027	Fries *et al.* [**?**]
(ρ-meson)		
Meson cloud	$= -6\int_0^1 g_1^p(x)dx \simeq -0.7$	Boreskov *et al.* [**?**]
($\pi-\rho$ interference)		
Meson cloud	$\simeq -0.004$ to -0.033	Cao *et al.* [**?**]
(ρ and $\pi-\rho$ interference)		
Meson cloud	< 0	Kumano *et al.* [**?**]
(ρ-meson)		
Meson cloud	$\simeq 0.12$	Fries *et al.* [**?**]
($\pi-\sigma$ interference)		
Pauli-blocking (bag model)	$\simeq 0.09$	Cao *et al.* [**?**]
Pauli-blocking (ansatz)	$\simeq 0.3$	Gluck *et al.* [**?**]
Pauli-blocking	$= \frac{5}{3}\int_0^1[\bar{d}(x)-\bar{u}(x)]dx \simeq 0.2$	Steffens [**?**]
Chiral-quark soliton	0.31	Dressler [**?**]
Chiral-quark soliton	$\simeq \int_0^1 2x^0.12[\bar{d}(x)-\bar{u}(x)]dx$	Wakamatsu *et al.* [**?**]
Instanton	$= \frac{5}{3}\int_0^1[\bar{d}(x)-\bar{u}(x)]dx \simeq 0.2$	Dorokhov [**?**]
Statistical	$\simeq \int_0^1[\bar{d}(x)-\bar{u}(x)]dx \simeq 0.12$	Bourrely *et al.* [**?**]
Statistical	$> \int_0^1[\bar{d}(x)-\bar{u}(x)]dx \simeq 0.12$	Bhalerao [**?**]

Table 2.1: A summary [**?**] of theoretical predictions of $I_\Delta = \int_0^1[\Delta\bar{u}(x) - \Delta\bar{d}(x)]dx$.

Chapter 3

The Experiment

3.1 Summary of Requested Beam Time Allocations

An experiment is proposed to measure the longitudinal virtual photon asymmetries A_{1h}^n in the SIDIS reaction on a longitudinally polarized ^{3}He target. The experiment will use a high-luminosity polarized ^{3}He target currently under development for several approved experiments, together with the BigBite [3, 4, 5] and Super BigBite [6, 7] spectrometers in Hall A. There are essentially five adjustable parameters of the experiment; the beam energy E_{beam}, the two spectrometer angles θ_{BB} and θ_{SBS}, and the target-magnet yoke distances d_{BB} and d_{SBS}. Table 3.1 shows the requested

Table 3.1: Requested beam time allocations. In total, 30 beam-days of production on ^{3}He and 3 beam-days for configuration changes and calibration measurements are requested. Production data collection is divided between beam energies of 11 GeV (20 days) and 8.8 GeV (10 days). At each beam energy, the beam time is divided equally between two SBS angle settings of 14 and 10 degrees. Calibrations include measurements on unpolarized ^{3}He, N_2, H_2 and empty reference cells for dilutions and multi-foil solid targets for spectrometer optics calibrations. E_{beam} is the beam energy, $\theta_{BB/SBS}$ is the spectrometer central angle and $d_{BB/SBS}$ is the distance from the center of the target to the front face of the magnet yoke along the spectrometer axis.

Beam days	Purpose	E_{beam} (GeV)	θ_{BB} (deg.)	θ_{SBS} (deg.)	d_{BB} (m)	d_{SBS} (m)
10	Production	11	30	14	1.55	2.5
10	Production	11	30	10	1.55	2.6
5	Production	8.8	30	14	1.55	2.5
5	Production	8.8	30	10	1.55	2.6
1	Calibration	11	30	14	1.55	2.5
1	Calibration	11	30	10	1.55	2.6
0.5	Calibration	8.8	30	14	1.55	2.5
0.5	Calibration	8.8	30	10	1.55	2.6
30	Total production					
3	Total calibrations					

beam allocations in each experiment configuration. The configuration of the spectrometers in the

proposed experiment is identical to that of the approved experiment E12-09-018 [8] in most respects. The main differences between the proposed experiment and E12-09-018 are:

- This proposal uses a longitudinally polarized ^{3}He target, whereas E12-09-018 will measure asymmetries on a transversely polarized target.
- The proposed experiment also includes data taking at a smaller SBS central angle of 10° to focus the hadron arm acceptance at smaller values of p_T^h, where the ϕ_h coverage is more complete and SIDIS cross sections are larger.

The double-spin asymmetries will be extracted with high statistical precision in a dense two-dimensional grid of (x, z) for $\pi^{\pm,0}$ and $K^{\pm}$, with $0.1 \leq x \leq 0.7$ and $0.2 \leq z \leq 0.8$. The data from two different SBS central angles will also provide a wide coverage in p_T^h and ϕ_h at the same x and z. Data at two different beam energies provide significantly different Q^2 values at the same x, leading to a "fully differential" mapping of the SIDIS asymmetries. However, since the main physics goal of this proposal is to provide data of high statistical precision for the flavor decomposition of the nucleon's longitudinal spin structure in the collinear approximation, the two-dimensional (x, z) kinematic binning is emphasized in this proposal.

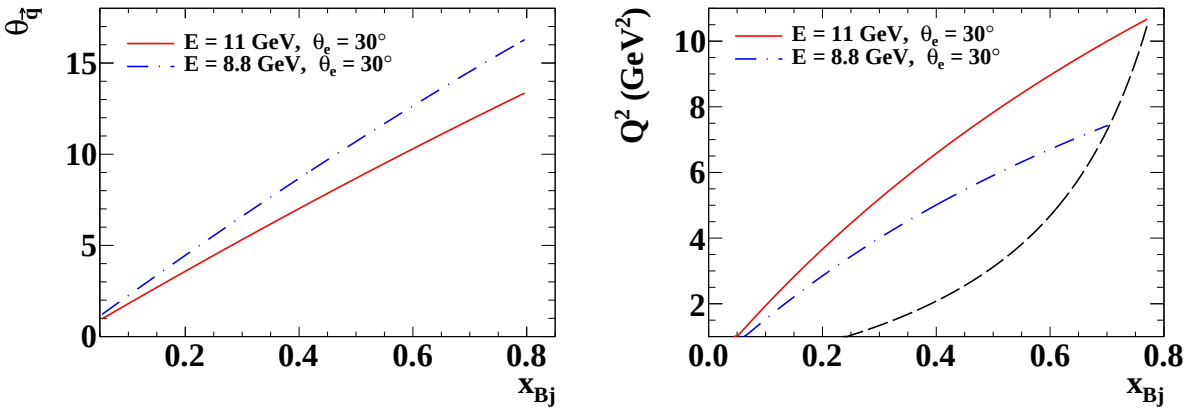

Figure 3.1: Left: Angle of the momentum transfer $\vec{q}$ relative to the beam direction vs x for an electron scattering angle $\theta_e = 30°$ and beam energies of 11 and 8.8 GeV. Right: Q^2 vs x at $\theta_e = 30°$ for 11 and 8.8 GeV. The black dashed curve shows the $W > 2$ GeV cutoff.

The motivation for taking roughly half the data at a smaller SBS central angle derives from the differences in physics goals between this proposal and E12-09-018. Figure 3.1 shows the direction of the momentum transfer $\vec{q}$ as a function of x at the central electron scattering angle of 30 degrees. In the absence of competing constraints, the optimal hadron arm angle coincides with the virtual photon direction $\theta_{\vec{q}}$. Since $\theta_{\vec{q}}$ varies as a function of x, the hadron arm acceptance can only be centered along $\vec{q}$ for a particular value of x. The transverse target single-spin asymmetries that will be measured by E12-09-018 vanish as $p_T^h \to 0$, such that the optimal SBS central angle is that which centers the SIDIS kinematic coverage at moderate, non-zero p_T^h. On the other hand, the longitudinal double-spin asymmetries used as input to the extraction of flavor-separated quark helicity distributions Δq do not vanish as $p_T^h \to 0$, so the optimal central angle of the hadron arm in this experiment is that which maximizes the SIDIS event rate for the $x - Q^2$ range covered by the electron arm. The potential benefit of moving to smaller SBS central angles is limited by the spatial constraints of the BigBite and SBS magnet and detector geometries and the downstream

beam pipe in Hall A; for a fixed position of BigBite, the minimum target-SBS magnet distance increases as the SBS central angle is reduced. Moreover, the detector background rates increase at smaller angles. The data obtained at two different SBS central angles will result in an overall increase in ϕ_h and p_T^h coverage and a significant increase in total statistics at lower x and p_T^h values.

3.2 Experiment Apparatus

In the proposed experiment, longitudinally polarized electron beams from CEBAF with energies of 11 and 8.8 GeV will collide with longitudinally polarized ^{3}He nuclei in a 60 cm-long target. A beam polarization of 85% is assumed throughout this proposal. This value for electron beam polarization has been routinely achieved and exceeded during the 6 GeV era of CEBAF operations. The beam current will be 40 μA on the 60-cm target at a pressure of 10.5 atm, leading to an effective electron-polarized-neutron luminosity of approximately 4×10^{36} cm^{-2} s^{-1}. Figure 3.2 shows the basic layout

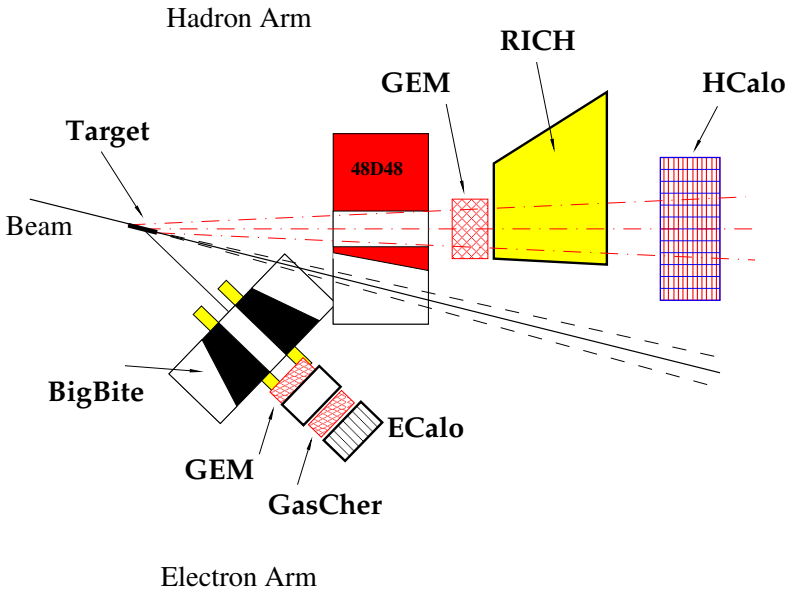

Figure 3.2: Schematic layout of the proposed measurements. The BigBite Spectrometer detects DIS electrons at a central angle of 30° on the beam right, while the Super BigBite Spectrometer detects SIDIS hadrons on the beam left in the vicinity of the momentum transfer direction at central angles of 14° and 10°.

of the experiment. BigBite will detect DIS electrons with momenta $p_e \geq 1$ GeV at a central angle of 30° on the beam right. Super BigBite (SBS) will detect SIDIS hadrons including $\pi^{\pm}$, π^0 and $K^{\pm}$ on the beam left, with data taking equally divided between central angles of 14° and 10°. The trigger threshold of the SBS hadronic calorimeter (HCAL) will be set for the efficient detection of hadrons with momentum $P_h \geq 2$ GeV.

The detector package of SBS will be oriented vertically behind the SBS magnet in the proposed experiment, leading to symmetric acceptances for positive and negative charged hadrons that are identical in first approximation. Moreover, the polarity of the SBS magnetic field will be periodically reversed, such that approximately half the data will be collected in up-bending and down-bending configurations for both positive and negative hadrons; the SBS polarity reversals will cancel the

effects of any residual differences in acceptance/efficiency between positive and negative hadrons, which will drastically reduce the systematic uncertainties in the charge-sum and charge-difference asymmetries. Reversing the SBS magnet polarity also increases the ϕ_h acceptance by roughly 14%, and the ϕ_h acceptance of the combination of upbending and downbending configurations is also symmetric about $\phi_h = 0$.

3.2.1 High-Luminosity Polarized ^{3}He Target

The operation of polarized ^{3}He targets at substantially higher luminosities than in previous experiments has been made possible by the recent development of targets using convection to more rapidly recirculate the ^{3}He gas from the optical pumping chamber in which it is polarized to the target cell in which it is exposed to the beam [9]. The ^{3}He target in the proposed experiment has the same basic operating parameters as the target to be used in E12-09-018 [8] and another approved SBS experiment E12-09-016 [10] that will measure the neutron electromagnetic form factor ratio G_E^n/G_M^n up to $Q^2 \sim 10$ GeV^2. The target will be 60 cm thick along the beam direction at a pressure of 10.5 atm. The use of thin metal end windows to reduce backgrounds will allow an increase in the useful luminosity by a factor of 3-4 while only increasing the total luminosity by roughly a factor of 2 compared to representative experiments from the 6 GeV era, such as the E06-010 experiment [11]. The target in the proposed experiment differs from the other two SBS ^{3}He experiments only in the orientation of the target polarization, which will be along the beam direction in this experiment. An in-beam ^{3}He polarization of 65% is assumed throughout this proposal in the calculation of projected asymmetry uncertainties.

3.2.2 BigBite Spectrometer

BigBite is a non-focusing magnetic spectrometer consisting of a vertical-bend dipole magnet with a maximum field-integral of approximately 1.0 T·m that can be instrumented with a flexible configuration of detectors. At its maximum field setting, the BigBite dipole bends the trajectory of a 1.5 GeV particle of charge e by approximately 10 degrees, providing for moderate momentum resolution of approximately 1% for charged-particle momenta up to several GeV. The BigBite spectrometer was first used at the NIKHEF facility [4, 3] and was later installed in Hall A at Jefferson Lab, where it has been successfully used in several different experiments, including but not limited to the measurement of the neutron electric form factor G_E^n up to $Q^2 = 3.4$ GeV^2 [12], SIDIS on a transversely polarized ^{3}He target [11] and many other experiments that have completed data taking but are not yet published. In the G_E^n and SIDIS experiments, BigBite was used as the electron spectrometer in coincidence with a hadron detector on the opposite side of the beamline. Following the 12 GeV upgrade, BigBite will be used in this role again in several approved experiments, including E12-09-016 [10] and E12-09-018 [8].

In order to tolerate the higher luminosities of planned experiments at 11 GeV, and to realize the improvements in tracking resolution needed to preserve the $\sim$ 1% momentum resolution of BigBite for higher-momentum particles at the same field integral, the BigBite drift chambers will be replaced with Gas Electron Multiplier (GEM) trackers [13, 14], which have been shown to have stable gain at charged-particle rates of up to 1 MHz/mm^2. A large number of GEM chambers are currently being produced at UVA and INFN for E12-07-109 [15], a measurement of the proton electromagnetic form factor ratio G_E^p/G_M^p to $Q^2 = 12$ GeV^2. The GEMs are modular in design, with an active area of up to 50×60 cm^2, and will be available to other experiments in Hall A when E12-07-109, which does not use BigBite, is not running. Another planned upgrade to the BigBite detector package for experiments at 11 GeV is a highly-segmented gas Cherenkov detector currently

under construction at the College of William and Mary, which will improve electron identification in BigBite compared to 6 GeV experiments that primarily used the lead-glass calorimeter for this purpose.

3.2.3 Super BigBite Spectrometer

The Super BigBite Spectrometer (SBS) [6, 7] is a device conceptually similar to BigBite. The SBS will use a "48D48" magnet acquired by JLab from BNL as a magnetic spectrometer, operated at a field integral of roughly 1.8 T·m. The SBS will be capable of reaching forward scattering angles by means of a cut in the magnet yoke for passage of the beam pipe. In E12-07-109, which proposed to run at luminosities approaching 10^{39} cm^{-2}s^{-1}, the SBS will be instrumented with a proton polarimeter constructed from GEM trackers and CH_2 analyzers, and a hadronic calorimeter for triggering on high-momentum protons. A significant challenge in the use of open-geometry spectrometers such as BigBite and SBS is the implementation of a trigger that is selective enough to reduce the data acquisition (DAQ) rate to a manageable level while maintaining high efficiency for the events of interest. The BigBite and SBS designs achieve this by exploiting the exponential decrease of the trigger rate as a function of the energy threshold in total-absorption calorimeters. Manageable trigger rates are achieved using a calorimeter-based coincidence trigger between two independent spectrometer arms, each with as high a threshold as the experiment physics goals and detector performance will allow.

All of the SBS experiments will make use of a hadronic calorimeter currently under construction at Carnegie Mellon University. The design of the calorimeter is very similar to that of the "HCAL1" detector used by the COMPASS experiment [16], but with several improvements needed to meet the performance specifications of the SBS experiments. The calorimeter consists of a 12×24 array of modules, each consisting of a stack of 40 alternating layers of 20 mm-thick iron and 5 mm-thick scintillator, with a frontal area of 15 × 15 cm^2. The design goals for HCAL include a high ($\gtrsim 95\%$) trigger efficiency for protons with momenta from roughly 3-8 GeV at a threshold of 25% of the average signal, a timing resolution of 1 ns or less, and a coordinate resolution better than 5 cm. To meet these requirements, the SBS HCAL will use fast scintillator and wavelength shifter materials and a novel light guide to collect the scintillation light onto two-inch-diameter PMTs with faster response time and higher quantum efficiency than those used by the COMPASS experiment. In E12-09-018, the SBS HCAL will be used as a charged hadron trigger and will also detect π^0s. A Monte Carlo evaluation of the π^0 acceptance and reconstruction efficiency in the SBS showed that the π^0 statistics will be similar to those of charged kaons.

Two different types of GEM trackers are being constructed for the SBS experiments. The SBS front tracker GEMs, currently under construction at INFN, consist of six tracker planes, each consisting of three 40×50 cm^2 GEM modules, arranged vertically for a total area per plane of 40×150 cm^2. In the G_E^p experiment, the front tracker is used to measure the kinematics of the scattered proton in elastic ep scattering and to define the incident proton trajectory before the polarization-analyzing scattering in CH_2. The front tracker GEMs are subject to the most stringent performance requirements because they are in direct view of the target at a luminosity of $\sim 8\times10^{38}$ cm^{-2} s^{-1}, and experience soft-photon-induced background hit rates of roughly 400 kHz/cm^2 [7]. To realize efficient track reconstruction capability with low false-positives in this environment, a spatial resolution of 70 μm is required. To realize this spatial resolution, a readout strip pitch of 0.4 mm in both directions is used, leading to a total of about 60,000 readout channels for the entire front tracker.

The SBS polarimeter GEMs, currently under construction at UVA, are subject to different and less stringent performance requirements. These GEMs are used to track protons scattered in

CH_2 analyzers. They are shielded from the target by the CH_2 analyzers and therefore have lower background rates than the front trackers. Only moderate spatial resolution is required for reliable tracking and sufficient resolution of the proton scattering angles in the CH_2 analyzers. Although the readout planes for the polarimeter GEMs have the same 0.4 mm strip pitch as the front tracker GEMs, the less demanding resolution requirement and the lower expected occupancy allow for two readout strips to be combined into a single readout channel to reduce the number of electronics channels required. On the other hand, a larger area is needed for the polarimeter GEMs in order to provide complete azimuthal acceptance for protons scattered by up to 10 degrees in the CH_2. A total of 40 GEM modules of area 50×60 cm^2 will be produced. These modules will be arranged into two trackers, each consisting of five planes of area 60×200 cm^2. The first polarimeter tracker will be located between the two CH_2 analyzers, while the second will be located between the second CH_2 analyzer and HCAL. In E12-09-018 and in the proposed experiment, GEM-based trackers for BigBite and SBS will be assembled from a combination of the front tracker and polarimeter GEM modules. Because the total luminosity in E12-09-018 is a factor of 40 lower than E12-07-109, the background environment in SBS is much more forgiving, such that a large-area tracker assembled from polarimeter GEM modules will have sufficient tracking performance and resolution.

3.2.4 Ring-Imaging Cherenkov detector for SBS

The designs of SBS and BigBite lend themselves naturally to the study of SIDIS at high x and Q^2. To make the SBS a viable hadron spectrometer for SIDIS requires a robust particle identification (PID) capability. The dual-radiator Ring-Imaging Cherenkov (RICH) detector from the HERMES experiment [17], which became available following the end of the HERMES experiment, was quickly recognized as an excellent low-cost solution for PID in the SBS. The HERMES RICH detector uses aerogel with a refractive index $n = 1.0304$ and C_4F_{10} gas with $n = 1.00137$ to provide redundant separation of pions, kaons and protons for momenta ranging from the kaon aerogel Cherenkov threshold of 2 GeV up to a limit of 15 GeV determined by the resolution of the reconstructed emission angle in the gas radiator. Cherenkov photons emitted by above-threshold charged hadrons in the aerogel and gas radiators are collected by a large-area spherical mirror with a radius of curvature of 2.2 m onto an array of 1,934 3/4"-diameter photomultiplier tubes (PMTs). The HERMES RICH consists of two identical detector halves on opposite sides of the HERA beam pipe in the HERMES spectrometer. One of the detector halves has been preserved and transferred to JLab for use in SBS, as well as the aerogel wall from the second half. Fig. 3.3 shows the basic design and working principle of the RICH. The aerogel wall consists of an array of 5 rows $\times$ 17 columns of aerogel tiles stacked 5 tiles deep. The average tile dimensions are $(11.4 \times 11.4 \times 1.13)$ cm^3.

Detailed Monte Carlo simulations of the HERMES RICH in SBS were carried out to determine the background rates in the PMTs and the useful acceptance of the RICH; i.e., the range of particle trajectories for which adequate PID performance is expected. Fig. 3.4 shows the layout of the RICH in the SBS Monte Carlo simulation using the GEANT4 toolkit [18], and examples of the Cherenkov light emitted by a pion and a kaon with identical trajectories. The simulation includes details of BigBite, the SBS magnet, the ^{3}He target, the GEM tracker, the RICH, HCAL, and the materials along the beamline. Preliminary background rate calculations for the PAC38 proposal for E12-09-018 [8] indicated an average PMT occupancy[1] of 0.1%, assuming the RICH PMT signals can be correlated in time with the signals from the other detectors to within ±5 ns. Such an occupancy leads to very high signal/noise ratios for the PID analysis. To achieve such a small effective timing

[1] "Occupancy" is defined as the probability of an accidental background hit within the timing window of an event.

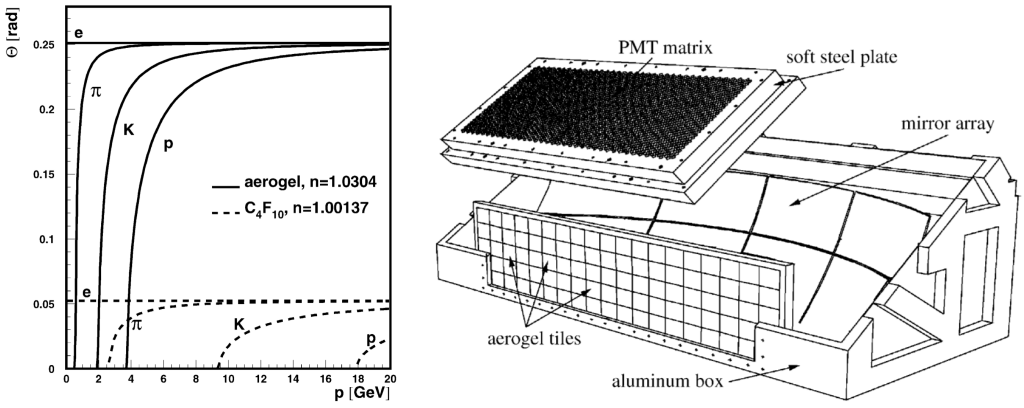

Figure 3.3: Left: Cherenkov emission angle θ as a function of particle momentum p for the dual-radiator HERMES RICH counter. Right: layout of the major components of the RICH. Figures reproduced from [17].

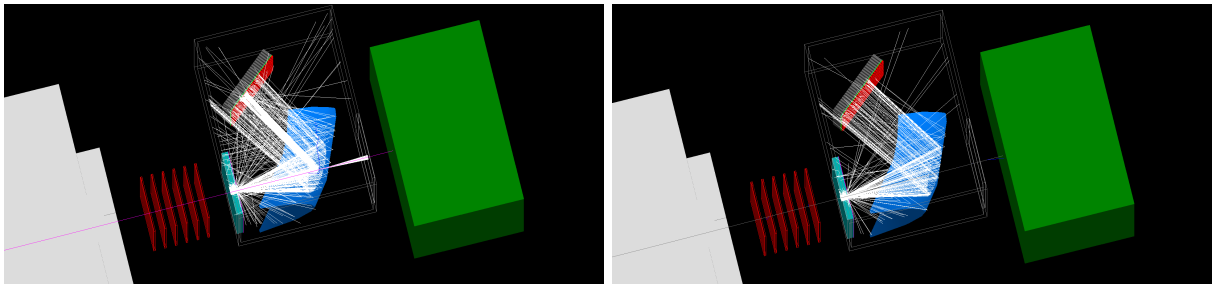

Figure 3.4: Layout of the HERMES RICH in the Monte Carlo simulation of E12-09-018. Left: A pion with a momentum of 5 GeV emits Cherenkov radiation in aerogel and gas. Right: A kaon moving along the same trajectory at the same momentum only produces Cherenkov light in aerogel at smaller emission angles. The spherical mirror collects the light onto the PMT matrix.

window requires the implementation of a TDC readout for the RICH PMTs in SBS, a feature which was absent from the HERMES setup because the beam repetition rate at HERA was such that the smallest useful time window for detector readout was 100 ns.

Fig. 3.5 shows preliminary PID results from the SBS RICH Monte Carlo simulation. The PID performance is characterized by the probability P_{ij} of assigning particle hypothesis j to a track with known true particle type i and reconstructed[2] momentum p. The PID assignment is made based on a simplified version of the inverse ray tracing algorithm described in [17]. The only requirement imposed on the selection of MC events for the PID analysis is the presence of a track, so that the misidentification probabilities shown include the effects of acceptance mismatch (i.e., those events which have small or non-existent signals because of a failure to produce and/or collect sufficient Cherenkov light). These preliminary results already demonstrate that the efficiency and purity of the PID analysis are high across the entire momentum range of interest, and that the geometry of the RICH does not significantly reduce the SBS acceptance relative to the combined acceptance of the SBS magnet and GEM tracker. Of particular importance is the low ($\lesssim 1\%$) probability to

[2]The momentum resolution of SBS is $\sigma_p/p \approx 1\%$.

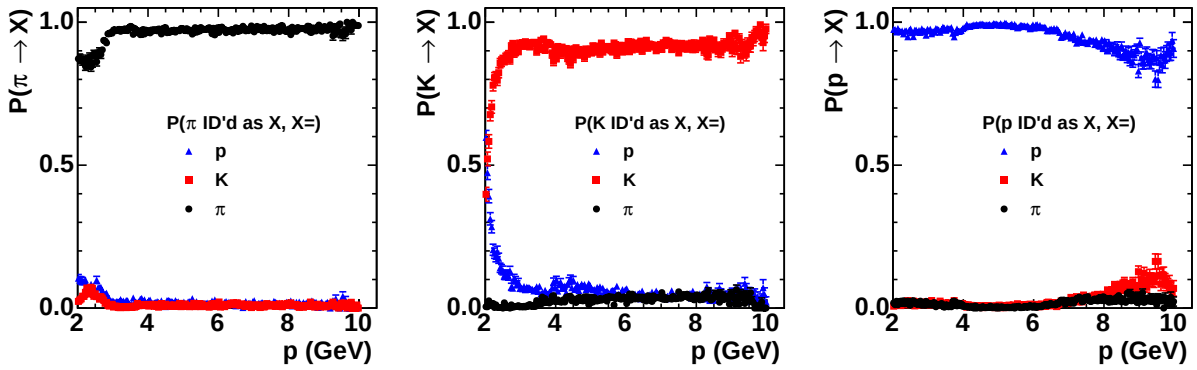

Figure 3.5: PID results from SBS Monte Carlo simulation. Particle ID probabilities as a function of momentum for pions (left), kaons (center) and protons (right). Results are preliminary and can be improved via further optimization of the PID algorithm.

misidentify pions as kaons above the pion gas threshold of ∼2.7 GeV, since the expected flux of pions is about ten times that of kaons in E12-09-018.

3.3 Experiment Plan and Expected Results

3.3.1 Monte Carlo Simulation

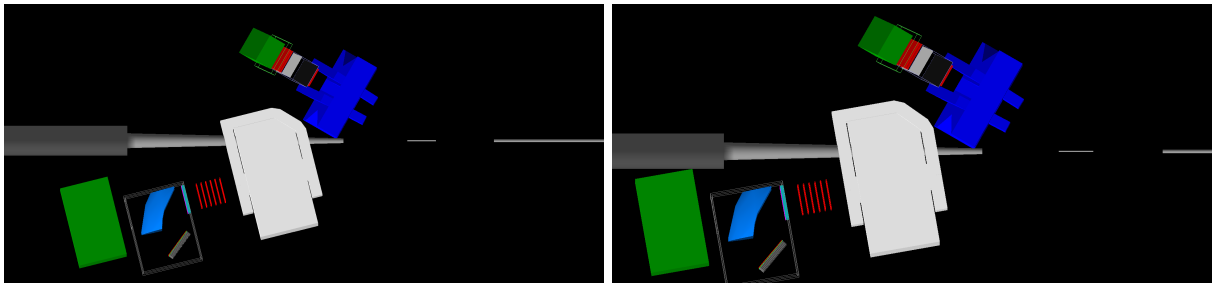

Figure 3.6: GEANT4 Monte Carlo model of the proposed experiment. Left: with SBS at a central angle of 14° at a distance of 2.5 meters, identical to approved experiment E12-09-018. Right: with SBS at a central angle of 10° at a distance of 2.6 meters.

Figure 3.6 shows the GEANT4 model of the proposed experiment in each of the two proposed SBS angle settings. The simulation includes the detailed geometries and field layouts of both magnets, the essential features of the ^{3}He target and the Hall A beamline, and realistic models of the detectors, which include the GEM tracker, the RICH and the HCAL for the hadron arm, and a GEM-based tracker, gas Cherenkov counter and electromagnetic calorimeter for the electron arm. SIDIS events were generated separately for each hadron species and propagated through the GEANT4 model. For all events, a good electron track in BigBite and above-threshold energy deposition in the BigBite calorimeter were required. For charged hadrons, a good track in SBS and above-threshold energy deposition in HCAL were required. The preliminary Monte Carlo studies of the RICH PID performance in SBS (see Fig. 3.5) already show that the acceptance of the RICH

does not significantly reduce the useful acceptance of SBS for high-performance PID, relative to the acceptance defined by the magnet gap and the tracker area. Therefore, because the GEANT4 simulation of Cherenkov radiation in the SBS RICH is computationally expensive, the RICH was not included in the analysis for rate estimates and asymmetry uncertainty projections. For π^0 events, both π^0 decay photons were required in HCAL with a minimum separation of one pixel. The following global cuts were applied to the "true" (nucleon rest frame) kinematics of generated SIDIS events:

- $Q^2 \geq 1$ GeV^2: Standard DIS cut.
- $W \geq 2$ GeV: Standard DIS cut to avoid the nucleon resonance region.
- $M_X \geq 1.5$ GeV: Large missing-mass cut to avoid the exclusive and resonance regions of $n(e,e'h)X$.
- $P_h \geq 2$ GeV: Minimum hadron momentum to minimize effects of nuclear final-state-interactions and target fragmentation.
- $y \leq 0.9$: Maximum fractional electron energy loss to avoid large QED radiative corrections, as well as large pair-production backgrounds present at low electron energies.
- $P_e \geq 1$ GeV: "Trigger threshold" for BigBite; redundant with y cut.

3.3.2 SIDIS Cross Section Model

For the purpose of rate estimation for this proposal, the unpolarized SIDIS cross section was calculated using a naive, leading-order, leading-twist approximation with the CTEQ6 PDFs [19] and the DSS2007 fragmentation functions [20] for pions and kaons, neglecting any ϕ_h dependence. The unpolarized differential scattering cross section is given in this simple model by

$$\frac{d\sigma}{dE'_e d\Omega_e dz dp_T^2 d\phi_h} = \frac{4\alpha^2 E'^2_e}{Q^4}\left[\frac{2H_1}{M}\sin^2\left(\frac{\theta_e}{2}\right) + \frac{H_2}{\nu}\cos^2\left(\frac{\theta_e}{2}\right)\right], \tag{3.1}$$

where E'_e is the scattered electron energy, M is the nucleon mass, θ_e is the electron scattering angle, ν is the electron energy loss in the target rest frame, and the SIDIS structure function H_2 is given at leading order by

$$H_2(x,Q^2,z,p_T^2) = x\sum_q e_q^2 q(x,Q^2) D_q^h(z,Q^2)\frac{b_q^h}{2\pi}e^{-b_q^h p_T^2}. \tag{3.2}$$

Six light quark flavors $q = u, d, s, \bar{u}, \bar{d}, \bar{s}$ are included in the sum. $q(x,Q^2)$ is the unpolarized PDF for quark flavor q and $D_h^q(z,Q^2)$ is the unpolarized fragmentation function for quark q to hadron h. A factorized Gaussian transverse momentum dependence is assumed, with a flavor-independent average width given by:

$$b_q^h = \frac{1}{z^2\left\langle k_\perp^2\right\rangle + \left\langle p_\perp^2\right\rangle}, \tag{3.3}$$

where $\left\langle k_\perp^2\right\rangle$ is the transverse momentum width of the initial quark distribution and $\left\langle p_\perp^2\right\rangle$ is the width of the transverse momentum distribution of hadrons produced in the fragmentation of the recoiling quark. For the purposes of rate estimates for this proposal, constant values $\left\langle k_\perp^2\right\rangle = 0.25$

GeV^2 and $\langle p_\perp^2 \rangle = 0.20$ GeV^2 were assumed, following Ref. [21]. The Callan-Gross relation $H_2 = 2xH_1$ is assumed for the SIDIS structure functions, implying neglect of the longitudinal virtual photoabsorbtion cross section. The kinematic coverages and rate estimates shown in the next sections correspond to the simplified SIDIS cross section model of Eqn. (3.1) convoluted with the combined acceptance of the two-spectrometer setup.

SIDIS events on ^{3}He "smeared" by the Fermi motion of the initial nucleons were generated in the GEANT4 simulation using the following procedure. First, the nucleon participating in the scattering event is chosen randomly; i.e., a neutron (proton) is chosen with probability $\frac{1}{3}$ ($\frac{2}{3}$). After choosing the initial nucleon, its initial momentum is sampled from the neutron (proton) momentum distribution in ^{3}He obtained from a fit to the results of a calculation using the Argonne V18 potential, and its initial direction of motion is chosen randomly. The polar ($\cos\theta_{e/h}$) and azimuthal ($\phi_{e/h}$) scattering angles and energies $E'_{e/h}$ of outgoing particles in the *lab frame* are generated randomly within limits chosen to populate the full solid angle and momentum acceptance of both spectrometers. The initial and final electron and nucleon four-momenta are then boosted to the nucleon rest frame, and the SIDIS cross section is computed using Eqn. (3.1). If the nucleon participating in the scattering is a neutron, the cross section is obtained from that on a proton by interchanging u and d quarks. The "true" (nucleon rest frame) SIDIS kinematics are also calculated. Finally, the lab-frame cross section is computed from the nucleon-rest-frame cross section by accounting for the modification of the flux factor by the boost due to the fact that the collision in the lab frame is no longer collinear[3]. The weight of each event is then calculated by multiplying the lab frame differential cross section by the Lorentz-invariant phase space volume of event generation and the integrated luminosity and dividing by the number of generated events. The weight thus defined represents the expected number of experimental counts corresponding to each Monte Carlo event. By keeping track of the identity of the nucleon participating in the collision, the dilution factors relating the ^{3}He asymmetry to the neutron asymmetry are also determined.

3.3.3 SIDIS Kinematic Coverage

Figure 3.7 shows the projected SIDIS $^3He(e,e'\pi^+)X$ yield as a function of the kinematic variables x, z, p_T^h and ϕ_h for each of the four beam energy/SBS angle configurations. The ten-degree setting exhibits higher event rates at low x and low p_T^h values and greater ϕ_h coverage than the 14-degree setting. On the other hand, for $x \gtrsim 0.5$ and $p_T^h \gtrsim 0.6$ GeV, the yield for the 14-degree setting equals or exceeds that of the 10-degree setting. In both settings, the ϕ_h coverage is peaked near $\phi_h \approx \pm\pi$, averages about half of 2π, and increases at low p_T^h/high x values.

Figure 3.8 shows the coverages of the SIDIS kinematic variables Q^2, z, p_T^h and ϕ_h as a function of x in each of the four proposed energy/angle combinations. The color scale of the plots corresponds to the expected total number of $^3He(e,e'\pi^+)X$ events in each bin. Q^2 is strongly correlated with x as a consequence of the large horizontal/vertical aspect ratio of the BigBite magnet gap. Due to the large momentum acceptance of both spectrometers, the z and x acceptances are largely uncorrelated, leading to a wide, independent range of x and z within a single angle/beam energy setting. The correlation between the momentum transfer direction and x leads to a weak negative correlation between p_T^h and x. The ϕ_h coverage increases with x for the same reason.

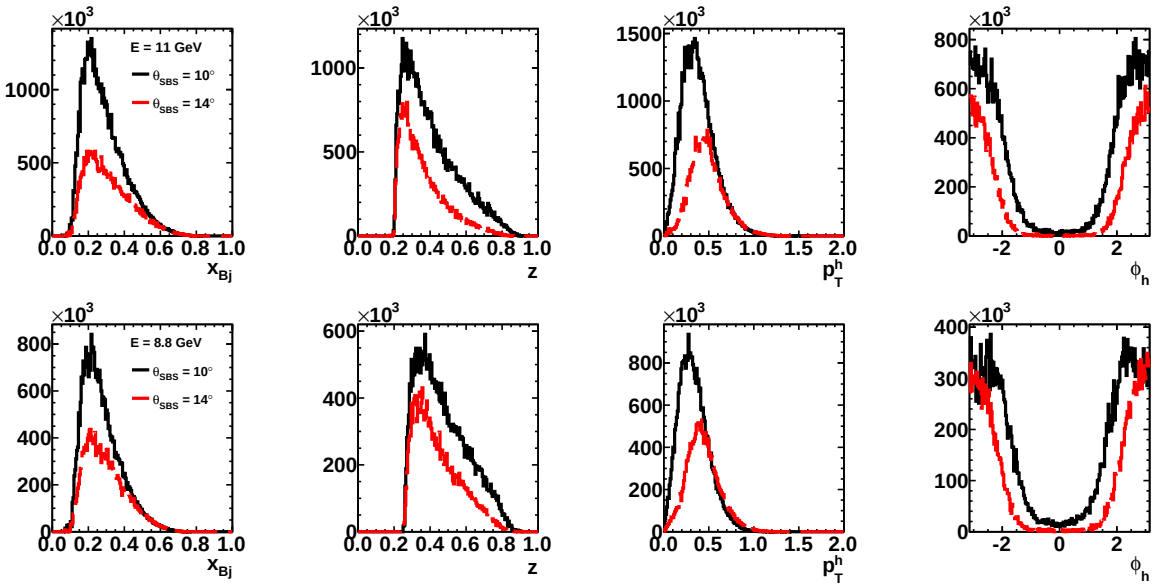

Figure 3.7: Expected distributions of the kinematic variables x, z, p_T^h and ϕ_h (from left to right) in $^3He(e,e'\pi^+)X$, for $E = 11$ GeV (top row) and $E = 8.8$ GeV (bottom row). Black solid (red dashed) lines are for $\theta_{SBS} = 10^\circ(14^\circ)$. The histograms are normalized so that the vertical axis corresponds to the total number of $^3He(e,e'\pi^+)X$ events in the beam time allocated to the configuration in question.

3.3.4 Event Rates

Table 3.2 shows the total SIDIS event rates for the five hadron species after applying kinematic cuts to select the SIDIS reaction in the current fragmentation region. Although the π^0 production rate is similar to the charged pion production rates[4], the SBS acceptance for π^0s is further reduced relative to the charged pion acceptance by the requirement that both π^0 decay photons are detected with a minimum separation of one pixel.

3.3.5 Projected Statistical Uncertainties in $A_{1h}^n(x,z)$

The experimentally observed double-spin asymmetry $A_{LL,h}^{exp}$ for hadron h on ^{3}He is approximately related to the longitudinal virtual photon asymmetry by:

$$A_{LL,h}^{exp} = P_B P_T A_{LL,h}^{^3He} = P_B P_T \mathcal{P}_{kin} A_{1h}^{^3He} = P_B P_T \mathcal{P}_{kin} \left[P_n f_n A_{1h}^n + P_p f_p A_{1h}^p \right], \quad (3.4)$$

where P_B and P_T are the beam and target polarizations, $P_n = 0.86^{+0.036}_{-0.02}$ and $P_p = -0.028^{+0.009}_{-0.004}$ are the neutron and proton effective polarizations in ^{3}He, $f_{n/p}$ is the "dilution" factor representing the fraction of the total ^{3}He SIDIS cross section carried by the neutron/protons, and $\mathcal{P}_{kin}$ is the kinematic factor appearing in Eqn. (2.3). This effective polarization approximation has been used for the extraction of neutron asymmetries from measured ^{3}He asymmetries by a number of previous experiments studying DIS on polarized ^{3}He targets [11, 22, 23]. The experimentally observed asymmetry is defined by the asymmetry in the measured SIDIS yield between events

[3]The flux factor $F \propto |\mathbf{v}_e - \mathbf{v}_N|$ is the only part of the cross section which is not Lorentz-invariant, but has the Lorentz transformation properties of a cross-sectional area.

[4]The π^0 fragmentation functions are assumed to be averages of π^+ and π^- (isospin symmetry assumption).

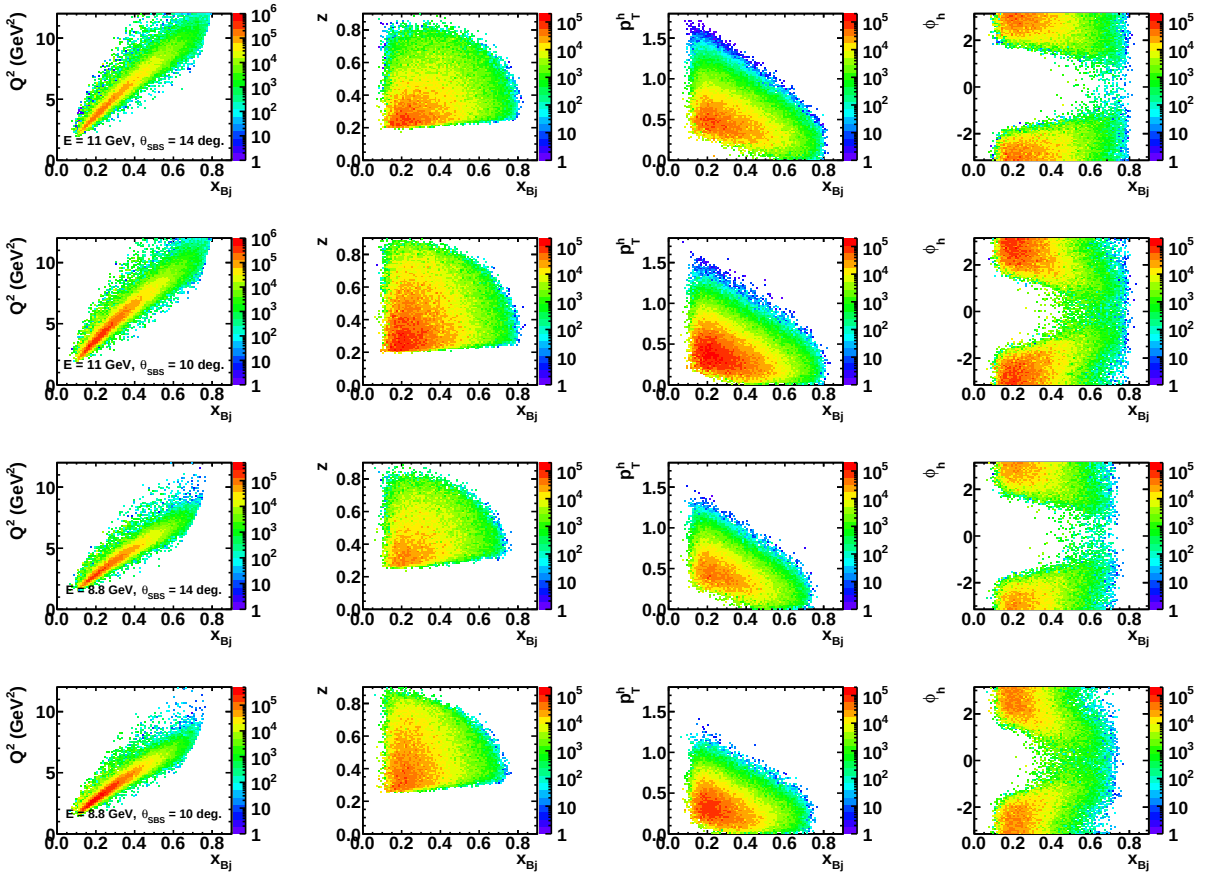

Figure 3.8: SIDIS phase space coverage of the four proposed experiment configurations for the ${}^3He(e,e'\pi^+)X$ channel. From left to right: Q^2, z, p_T^h and ϕ_h vs x. From top to bottom: $E = 11$ GeV, $\theta_{SBS} = 14^\circ$, $E = 11$ GeV, $\theta_{SBS} = 10^\circ$, $E = 8.8$ GeV, $\theta_{SBS} = 14^\circ$, and $E = 8.8$ GeV, $\theta_{SBS} = 10^\circ$. Color scale corresponds to the expected total number of events.

obtained with beam and target polarizations parallel and anti-parallel. Defining $N_+ \equiv N_{++} + N_{--}$ and $N_- \equiv N_{+-} + N_{-+}$ as the total SIDIS yields in parallel and anti-parallel conditions, respectively, the observed asymmetry is then defined as:

$$A_{LL,h}^{exp} = \frac{N_+ - N_-}{N_+ + N_-} \tag{3.5}$$

The statistical uncertainty in $A_{LL,h}^{exp}$ is given by

$$\Delta A_{LL,h}^{exp} = \sqrt{\frac{1 - (A_{LL,h}^{exp})^2}{N}}, \tag{3.6}$$

where $N \equiv N_+ + N_-$ is the total number of events. The projected uncertainty in A_{1h}^n for each (x, z) bin was estimated from equations (3.6) and (3.4). For the ratio $R = \sigma_L/\sigma_T$ that enters the kinematic factor $\mathcal{P}_{kin}$ of equation (2.3), the SLAC R1998 parametrization of inclusive DIS data was used [24], which implies the assumption, in the absence of data for R in SIDIS, that $R_{SIDIS} = R_{DIS}$. In the estimation of ΔA_{1h}^n for this proposal, the small A_{1h}^p correction due to the small but non-zero

Table 3.2: Expected total SIDIS $^3He(e,e'h)X$ event rates passing all SIDIS kinematic cuts: $Q^2 \geq 1$ GeV^2, $W \geq 2$ GeV, $M_X \geq 1.5$ GeV, $y \leq 0.9$, $P_h \geq 2$ GeV, $p_e \geq 1$ GeV.

Channel	$E = 11$ GeV $\theta_{SBS} = 14^\circ$	$E = 11$ GeV $\theta_{SBS} = 10^\circ$	$E = 8.8$ GeV $\theta_{SBS} = 14^\circ$	$E = 8.8$ GeV $\theta_{SBS} = 10^\circ$
$^3He(e,e'\pi^+)X$ rate (Hz)	35.5	69.9	47.1	78.3
$^3He(e,e'\pi^-)X$ rate (Hz)	23.4	43.8	28.8	45.7
$^3He(e,e'\pi^0)X$ rate (Hz)	4.8	11.1	6.4	11.0
$^3He(e,e'K^+)X$ rate (Hz)	5.8	12.6	8.7	15.2
$^3He(e,e'K^-)X$ rate (Hz)	1.1	2.4	1.4	2.4

proton polarization in ^{3}He was neglected. This correction will be well-constrained by existing data from HERMES as well as from future JLab measurements in CLAS12, and its contribution to the systematic uncertainty in A_{1n}^n will be small.

For the analysis of projected physics results, Monte-Carlo generated SIDIS events passing all cuts were subdivided into a two-dimensional rectangular grid of (x,z) bins in the range $(0.1 \leq x \leq 0.8, 0.2 \leq z \leq 0.8)$ with bin widths of $(\Delta x, \Delta z) = (0.1, 0.1)$. In each bin, the total number of events and the weighted-average kinematics $< x >$, $< Q^2 >$, $< z >$ and $< p_T^h >$ were calculated as well as the kinematic factor $< \mathcal{P}_{kin} >$ and the dilution factor f_n. The uncertainty ΔA_{1h}^n was then calculated in each bin using

$$\Delta A_{1h}^n = \frac{1}{P_B P_T f_n P_n \mathcal{P}_{kin} \sqrt{N}}, \tag{3.7}$$

where again the small A_{1h}^p correction has been neglected.

Figures 3.9-3.13 show the projected statistical uncertainties $\Delta A_{1h}^n(x,z)$ for the combined data from both SBS angle settings of the proposed experiment at 11 GeV beam energy, as a function of x in each z bin, compared to the predictions of the "DSSV+" NLO global QCD analysis of the DSSV group [25], which expanded the 2008 "DSSV" analysis [2, 26] to include subsequent data from the COMPASS collaboration on longitudinal spin asymmetries in μp and μd SIDIS [27, 28]. The curves showing the predicted neutron asymmetries in each kinematic bin are obtained via trilinear interpolation of a three dimensional grid of predicted values in (x, z, Q^2), kindly provided by the authors of [25].

3.3.6 Comparison to Existing Data

3.3.7 Comparison to Other Approved Experiments

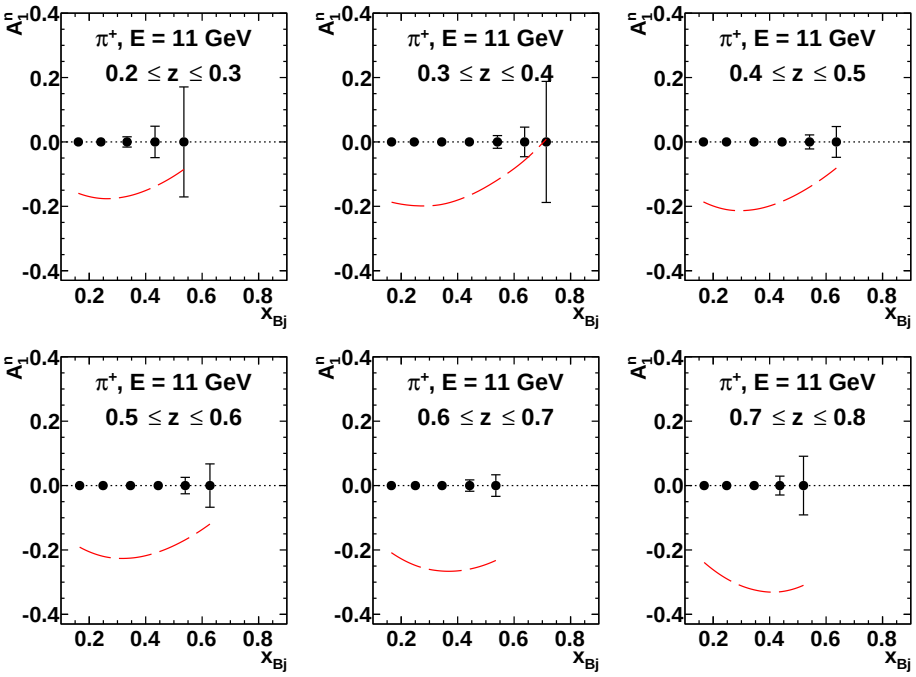

Figure 3.9: Projected uncertainties in $A^n_{1,\pi^+}(x,z)$ from combined 11 GeV running at both SBS angle settings, compared to the predictions of the recent NLO global QCD analysis of DSSV [25]

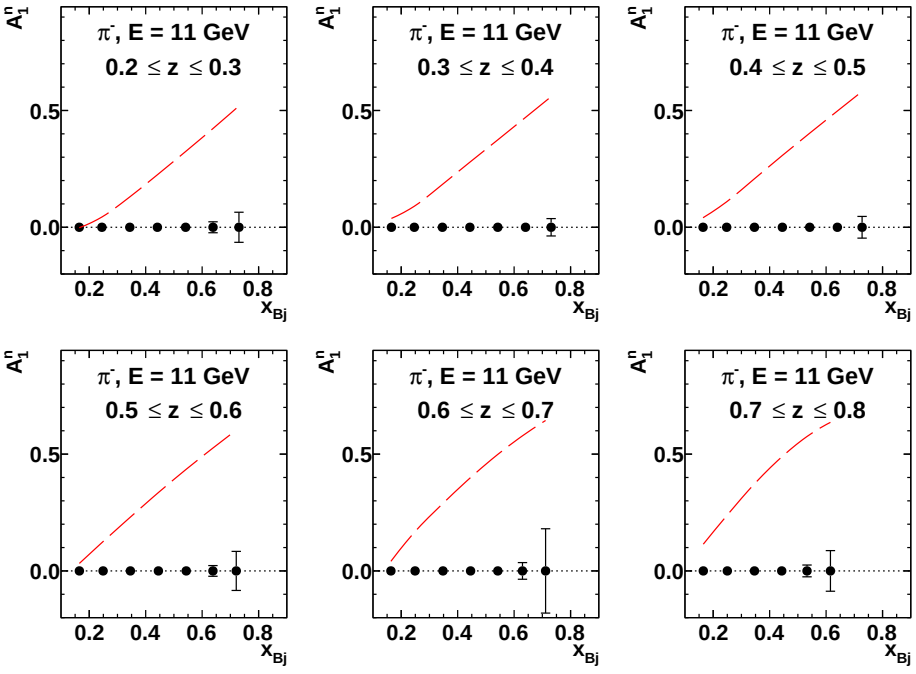

Figure 3.10: Projected uncertainties in $A^n_{1,\pi^-}(x,z)$ from combined 11 GeV running at both SBS angle settings, compared to the predictions of the recent NLO global QCD analysis of DSSV [25]

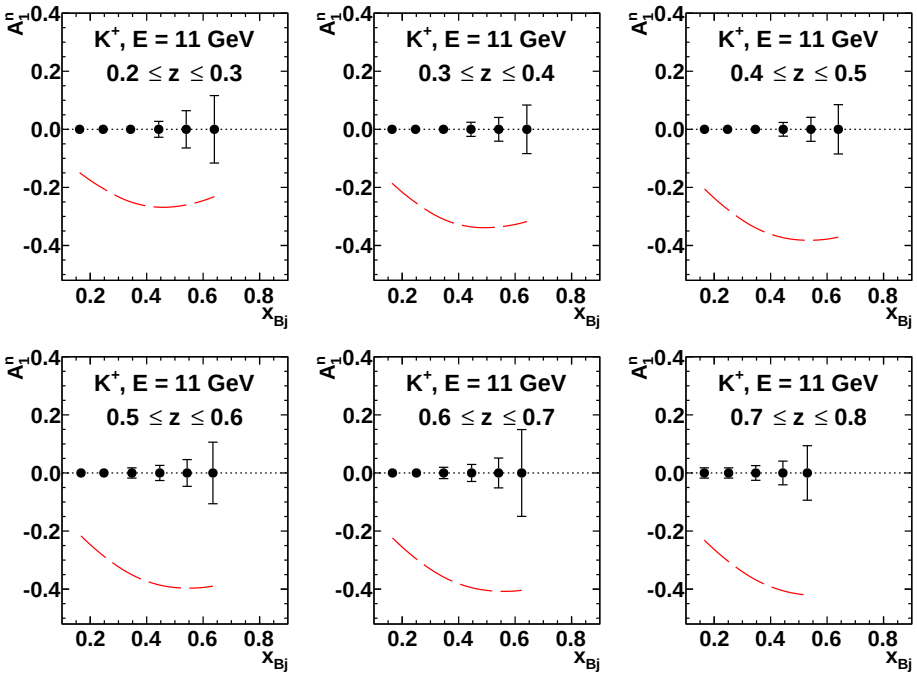

Figure 3.11: Projected uncertainties in $A^n_{1,K^+}(x,z)$ from combined 11 GeV running at both SBS angle settings, compared to the predictions of the recent NLO global QCD analysis of DSSV [25]

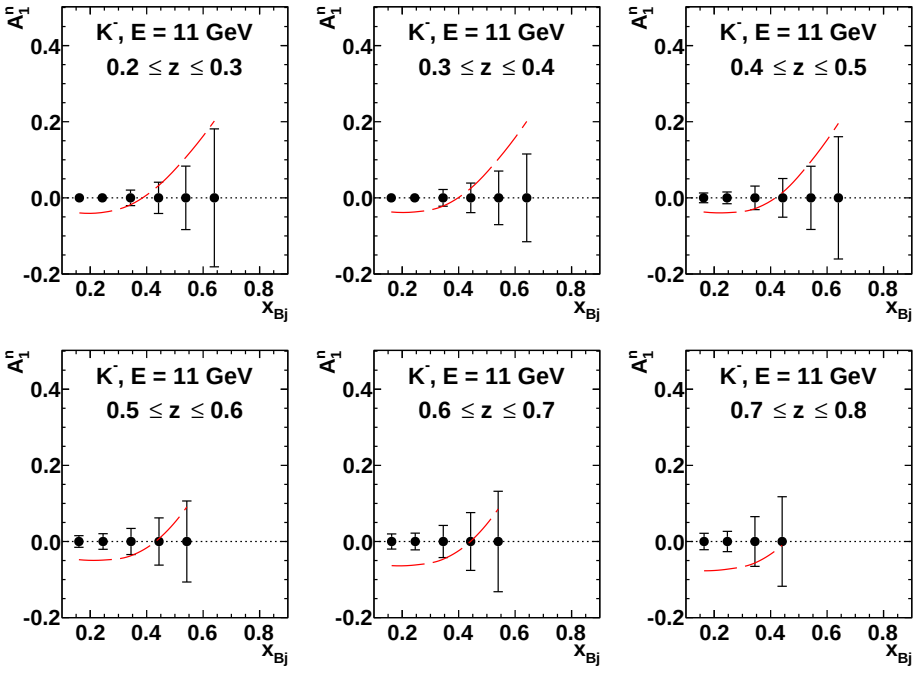

Figure 3.12: Projected uncertainties in $A^n_{1,K^-}(x,z)$ from combined 11 GeV running at both SBS angle settings, compared to the predictions of the recent NLO global QCD analysis of DSSV [25]

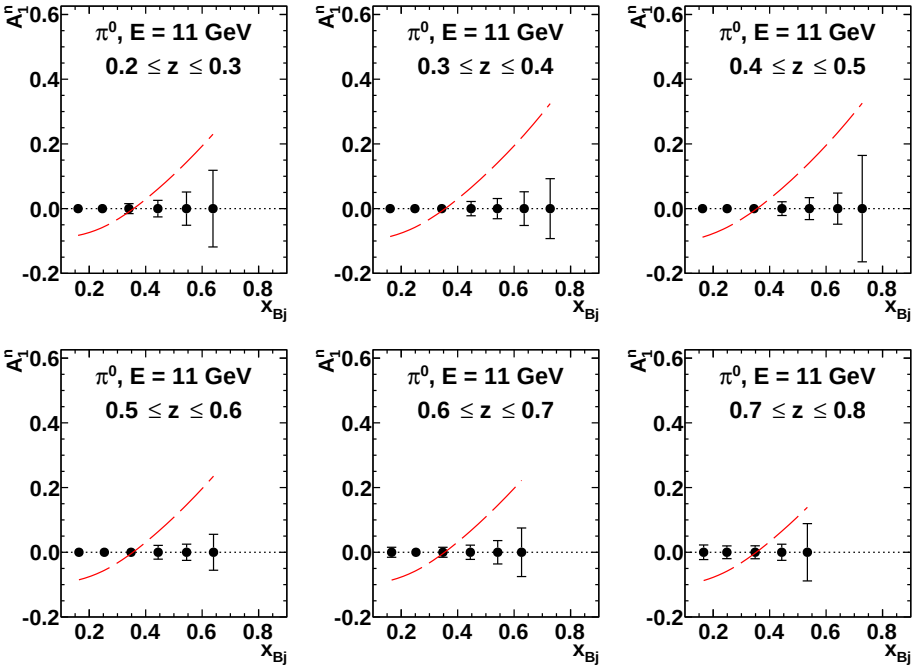

Figure 3.13: Projected uncertainties in $A^n_{1,\pi^0}(x,z)$ from combined 11 GeV running at both SBS angle settings, compared to the predictions of the recent NLO global QCD analysis of DSSV [25]

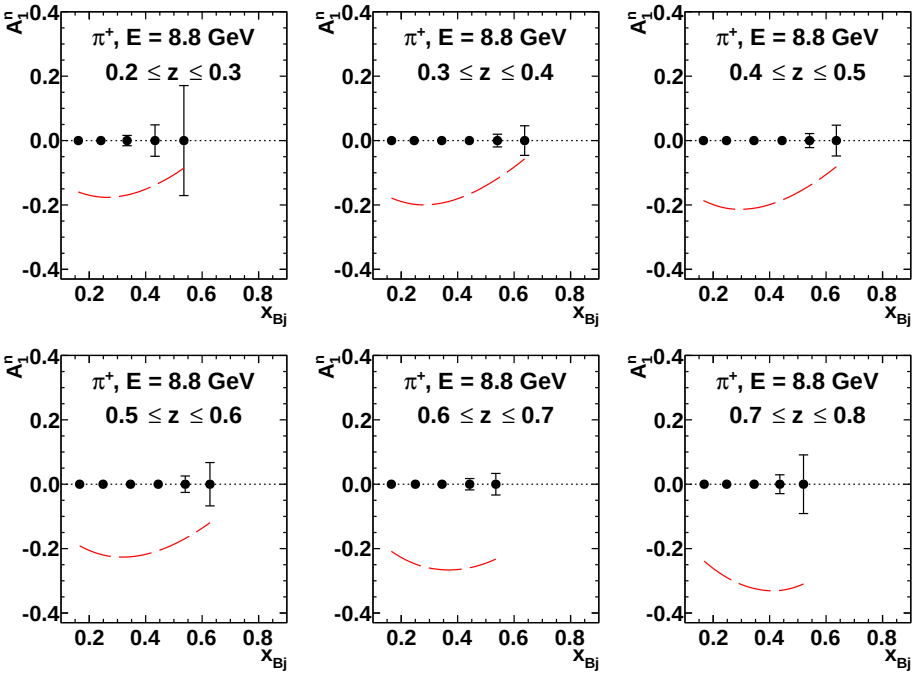

Figure 3.14: Projected uncertainties in $A^n_{1,\pi^+}(x,z)$ from combined 8.8 GeV running at both SBS angle settings, compared to the predictions of the recent NLO global QCD analysis of DSSV [25]

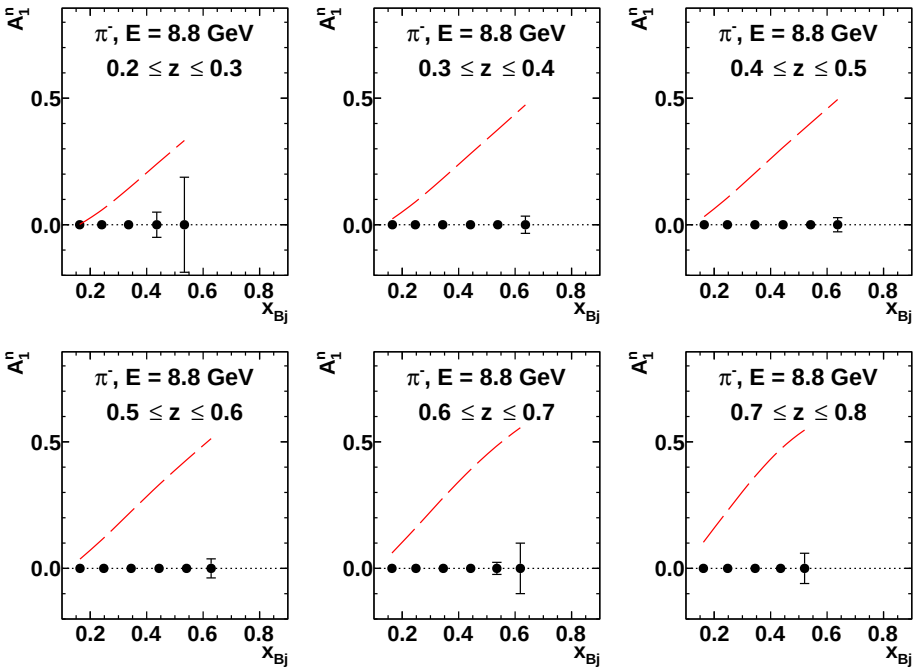

Figure 3.15: Projected uncertainties in $A^n_{1,\pi^-}(x,z)$ from combined 8.8 GeV running at both SBS angle settings, compared to the predictions of the recent NLO global QCD analysis of DSSV [25]

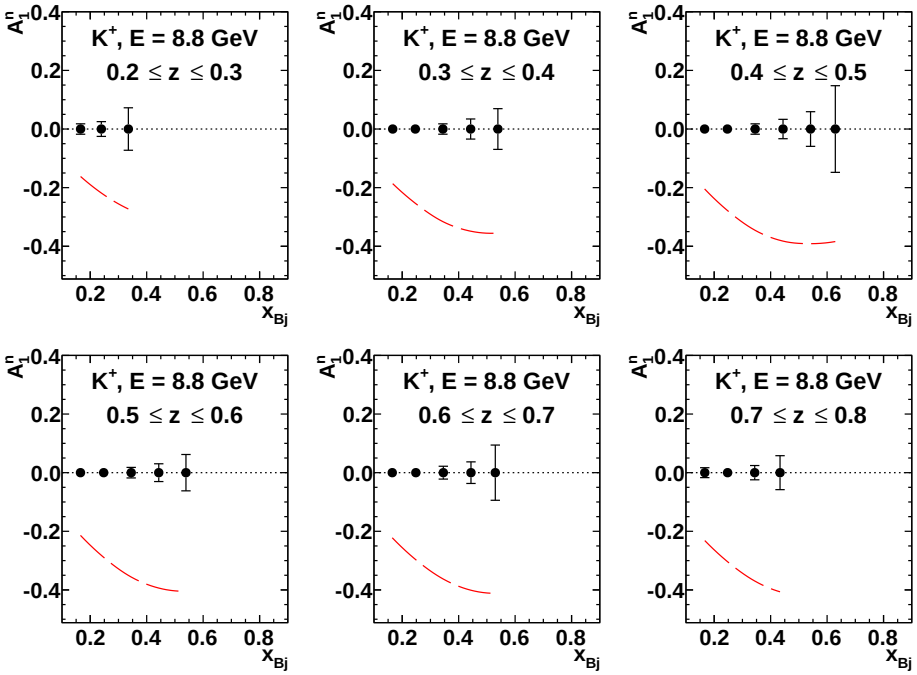

Figure 3.16: Projected uncertainties in $A^n_{1,K^+}(x,z)$ from combined 8.8 GeV running at both SBS angle settings, compared to the predictions of the recent NLO global QCD analysis of DSSV [25]

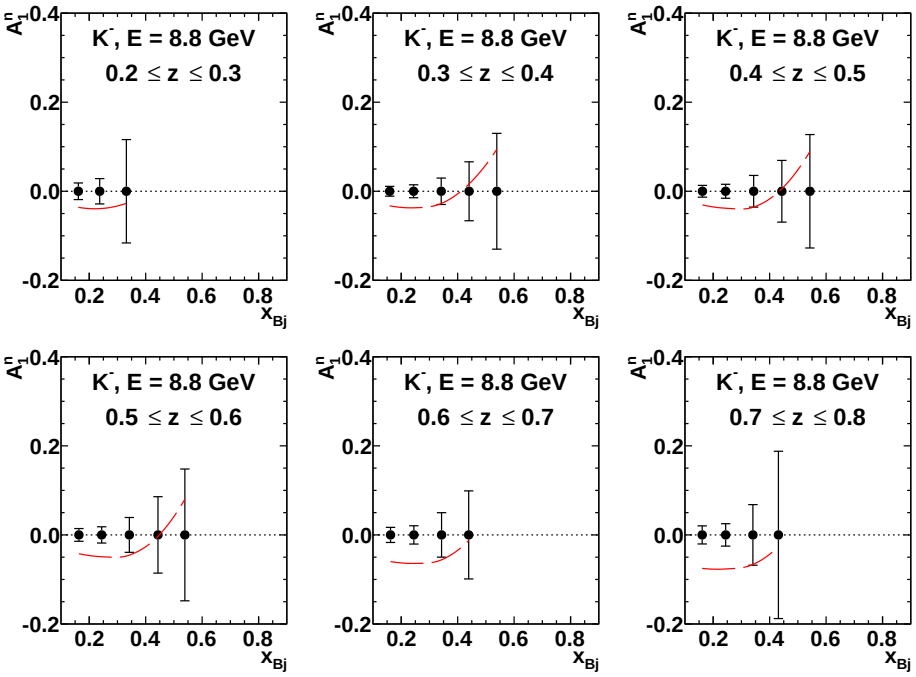

Figure 3.17: Projected uncertainties in $A^n_{1,K^-}(x,z)$ from combined 8.8 GeV running at both SBS angle settings, compared to the predictions of the recent NLO global QCD analysis of DSSV [25]

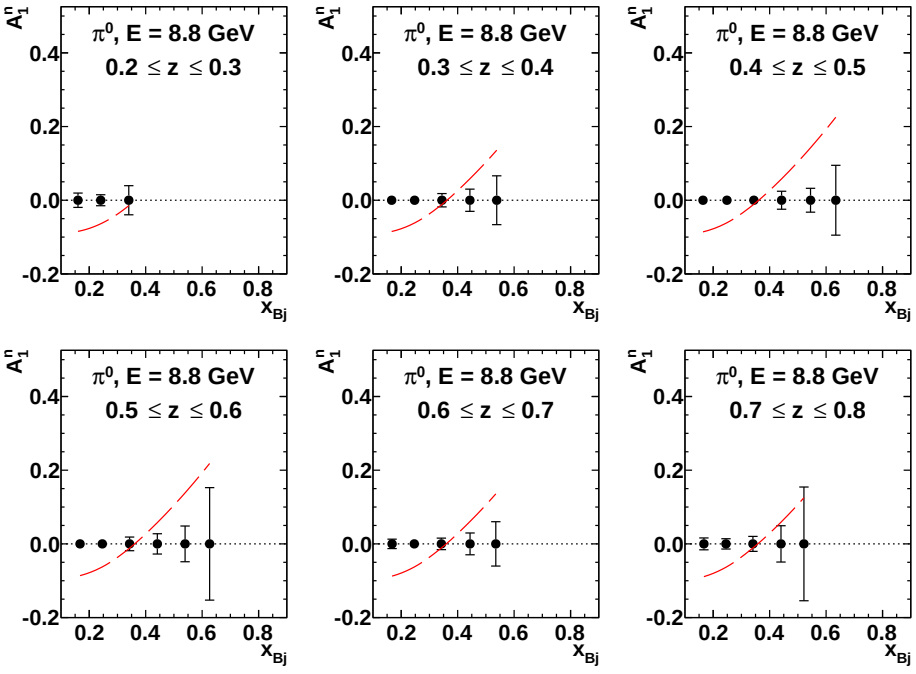

Figure 3.18: Projected uncertainties in $A^n_{1,\pi^0}(x,z)$ from combined 8.8 GeV running at both SBS angle settings, compared to the predictions of the recent NLO global QCD analysis of DSSV [25]

References

[1] L. Adamczyk et al. Measurement of longitudinal spin asymmetries for weak boson production in polarized proton-proton collisions at RHIC. 2014. arXiv:1404.6880.

[2] Daniel de Florian, Rodolfo Sassot, Marco Stratmann, and Werner Vogelsang. Global analysis of helicity parton densities and their uncertainties. *Phys. Rev. Lett.*, 101:072001, Aug 2008. URL: http://link.aps.org/doi/10.1103/PhysRevLett.101.072001, doi:10.1103/PhysRevLett.101.072001.

[3] D.J.J.de Lange et al. The optical properties of the bigbite spectrometer at {NIKHEF}. *Nuclear Instruments and Methods in Physics Research Section A: Accelerators, Spectrometers, Detectors and Associated Equipment*, 412(23):254 – 264, 1998. URL: http://www.sciencedirect.com/science/article/pii/S0168900298004768, doi:http://dx.doi.org/10.1016/S0168-9002(98)00476-8.

[4] D.J.J de Lange, J.J.M Steijger, H de Vries, M Anghinolfi, M Taiuti, D.W Higinbotham, B.E Norum, and E Konstantinov. A large acceptance spectrometer for the internal target facility at {NIKHEF}. *Nuclear Instruments and Methods in Physics Research Section A: Accelerators, Spectrometers, Detectors and Associated Equipment*, 406(2):182 – 194, 1998. URL: http://www.sciencedirect.com/science/article/pii/S0168900298919817, doi:http://dx.doi.org/10.1016/S0168-9002(98)91981-7.

[5] M. Mihovilovi et al. Methods for optical calibration of the bigbite hadron spectrometer. *Nuclear Instruments and Methods in Physics Research Section A: Accelerators, Spectrometers, Detectors and Associated Equipment*, 686(0):20 – 30, 2012. URL: http://www.sciencedirect.com/science/article/pii/S0168900212004901, doi:http://dx.doi.org/10.1016/j.nima.2012.04.085.

[6] J. J. LeRose, B. Wojtsekhowski, et al. The Super-Bigbite Spectrometer for Jefferson Lab Hall A. https://userweb.jlab.org/%7Ebogdanw/SBS-CDR/SBS-CDR.pdf, 2009.

[7] J. J. LeRose, B. Wojtsekhowski, et al. The Super-Bigbite Spectrometer for Jefferson Lab Hall A. https://userweb.jlab.org/~mahbub/HallA/SBS/SBS-CDR_New.pdf, 2010.

[8] G. Cates, E. Cisbani, G. Franklin, A. Puckett, B. Wojtsekhowski, et al. Target Single-Spin Asymmetries in Semi-Inclusive Pion and Kaon Electroproduction on a Transversely Polarized ^{3}He Target using Super BigBite and BigBite in Hall A. http://www.jlab.org/exp_prog/PACpage/PAC38/proposals/Conditionally%20Approved/C12-09-018_Update.pdf, 2011.

[9] P.A.M. Dolph, J. Singh, T. Averett, A. Kelleher, K.E. Mooney, et al. Gas dynamics in high-luminosity polarized He-3 targets using diffusion and convection. *Phys.Rev.*, C84:065201, 2011. arXiv:1107.1902, doi:10.1103/PhysRevC.84.065201.

[10] G. Cates, S. Riordan, B. Wojtsekhowski, et al. Measurement of the Neutron Electromagnetic Form Factor Ratio G_E^n/G_M^n at High Q^2. http://hallaweb.jlab.org/collab/PAC/PAC34/PR-09-016-gen.pdf, 2009.

[11] X. Qian et al. Single spin asymmetries in charged pion production from semi-inclusive deep inelastic scattering on a transversely polarized ^{3}He target at $Q^2 = 1.4\tilde{}2.7$ gev^2. *Phys. Rev. Lett.*, 107:072003, Aug 2011. URL: http://link.aps.org/doi/10.1103/PhysRevLett.107.072003, doi:10.1103/PhysRevLett.107.072003.

[12] S. Riordan et al. Measurements of the electric form factor of the neutron up to $q^2 = 3.4$ gev^2 using the reaction $^3he[over \rightarrow](e[over \rightarrow], e^{'}n)pp$. *Phys. Rev. Lett.*, 105(26):262302, Dec 2010. doi:10.1103/PhysRevLett.105.262302.

[13] F. Sauli. Gem: A new concept for electron amplification in gas detectors. *Nuclear Instruments and Methods in Physics Research Section A: Accelerators, Spectrometers, Detectors and Associated Equipment*, 386(23):531 – 534, 1997. URL: http://www.sciencedirect.com/science/article/pii/S0168900296011722, doi:http://dx.doi.org/10.1016/S0168-9002(96)01172-2.

[14] A Bressan, J.C Labb, P Pagano, L Ropelewski, and F Sauli. Beam tests of the gas electron multiplier. *Nuclear Instruments and Methods in Physics Research Section A: Accelerators, Spectrometers, Detectors and Associated Equipment*, 425(12):262 – 276, 1999. URL: http://www.sciencedirect.com/science/article/pii/S0168900298014065, doi:http://dx.doi.org/10.1016/S0168-9002(98)01406-5.

[15] E. Brash, E. Cisbani, M. Jones, M. Khandaker, L. Pentchev, C. F. Perdrisat, V. Punjabi, B. Wojtsekhowski, et al. Large Acceptance Proton Form Factor Ratio Measurements at 13 and 15 GeV^2 Using Recoil Polarization Method. http://www.jlab.org/exp_prog/proposals/07/PR12-07-109.pdf, 2007.

[16] N.V. Vlasov et al. A calorimeter for detecting hadrons with energies of 10100 gev. *Instruments and Experimental Techniques*, 49(1):41–55, 2006. URL: http://dx.doi.org/10.1134/S0020441206010040, doi:10.1134/S0020441206010040.

[17] N Akopov et al. The {HERMES} dual-radiator ring imaging cherenkov detector. *Nuclear Instruments and Methods in Physics Research Section A: Accelerators, Spectrometers, Detectors and Associated Equipment*, 479(23):511 – 530, 2002. URL: http://www.sciencedirect.com/science/article/pii/S0168900201009329, doi:http://dx.doi.org/10.1016/S0168-9002(01)00932-9.

[18] S. Agostinelli et al. Geant4a simulation toolkit. *Nuclear Instruments and Methods in Physics Research Section A: Accelerators, Spectrometers, Detectors and Associated Equipment*, 506(3):250 – 303, 2003. URL: http://www.sciencedirect.com/science/article/pii/S0168900203013688, doi:http://dx.doi.org/10.1016/S0168-9002(03)01368-8.

[19] W.K. Tung, H.L. Lai, A. Belyaev, J. Pumplin, D. Stump, et al. Heavy Quark Mass Effects in Deep Inelastic Scattering and Global QCD Analysis. *JHEP*, 0702:053, 2007. arXiv:hep-ph/0611254, doi:10.1088/1126-6708/2007/02/053.

[20] Daniel de Florian, Rodolfo Sassot, and Marco Stratmann. Global analysis of fragmentation functions for pions and kaons and their uncertainties. *Phys.Rev.*, D75:114010, 2007. arXiv:hep-ph/0703242, doi:10.1103/PhysRevD.75.114010.

[21] M. Anselmino, M. Boglione, U. D'Alesio, A. Kotzinian, F. Murgia, and A. Prokudin. Role of cahn and sivers effects in deep inelastic scattering. *Phys. Rev. D*, 71:074006, Apr 2005. URL: http://link.aps.org/doi/10.1103/PhysRevD.71.074006, doi:10.1103/PhysRevD.71.074006.

[22] J. Huang et al. *Phys.Rev.Lett.*, 108:052001, 2012. arXiv:1108.0489, doi:10.1103/PhysRevLett.108.052001.

[23] X. Zheng et al. Precision measurement of the neutron spin asymmetrya1n and spin-flavor decomposition in the valence quark region. *Phys. Rev. Lett.*, 92:012004, Jan 2004. URL: http://link.aps.org/doi/10.1103/PhysRevLett.92.012004, doi:10.1103/PhysRevLett.92.012004.

[24] K. Abe et al. *Physics Letters B*, 452(12):194 – 200, 1999. URL: http://www.sciencedirect.com/science/article/pii/S0370269399002440, doi:http://dx.doi.org/10.1016/S0370-2693(99)00244-0.

[25] D. de Florian, R. Sassot, M. Stratmann, and W. Vogelsang. Global analysis of helicity PDFs: Past - present - future. 2011. arXiv:1108.3955.

[26] Daniel de Florian, Rodolfo Sassot, Marco Stratmann, and Werner Vogelsang. Extraction of spin-dependent parton densities and their uncertainties. *Phys. Rev. D*, 80:034030, Aug 2009. URL: http://link.aps.org/doi/10.1103/PhysRevD.80.034030, doi:10.1103/PhysRevD.80.034030.

[27] M. Alekseev et al. Flavour Separation of Helicity Distributions from Deep Inelastic Muon-Deuteron Scattering. *Phys.Lett.*, B680:217–224, 2009. arXiv:0905.2828, doi:10.1016/j.physletb.2009.08.065.

[28] M.G. Alekseev et al. Quark helicity distributions from longitudinal spin asymmetries in muon-proton and muon-deuteron scattering. *Phys.Lett.*, B693:227–235, 2010. arXiv:1007.4061, doi:10.1016/j.physletb.2010.08.034.